
Research Articles: Systems/Circuits

Spontaneous Spiking Is Governed By Broadband Fluctuations

<https://doi.org/10.1523/JNEUROSCI.1899-21.2022>

Cite as: J. Neurosci 2022; 10.1523/JNEUROSCI.1899-21.2022

Received: 19 September 2021

Revised: 26 April 2022

Accepted: 28 April 2022

This Early Release article has been peer-reviewed and accepted, but has not been through the composition and copyediting processes. The final version may differ slightly in style or formatting and will contain links to any extended data.

Alerts: Sign up at www.jneurosci.org/alerts to receive customized email alerts when the fully formatted version of this article is published.

1 **Title: Spontaneous Spiking Is Governed By Broadband Fluctuations**

2 **Abbreviated Title: Spiking Is Governed By Broadband Fluctuations**

3 **Authors:** Zachary W. Davis¹, Lyle Muller^{2,3}, John Reynolds¹

4 **Affiliations:**

5 ¹The Salk Institute for Biological Studies, La Jolla, CA, USA. 92037

6 ²Department of Applied Mathematics, Western University, London, ON, Canada. N6A 3K7

7 ³Brain and Mind Institute, Western University, London, ON, Canada. N6A 3K7

8 Corresponding authors J.R. and Z.W.D., emails: reynolds@salk.edu and zdavis@salk.edu

9 **Pages:** 46

10 **Figures:** 7

11 **No. Words:** Abstract: 245; Introduction: 1472; Discussion: 1405

12 **Conflicts of Interest:** The authors declare no competing financial interests

13 **Acknowledgments:** Funding: Gatsby Charitable Foundation, the Fiona and Sanjay Jha Chair in
14 Neuroscience, the Canadian Institute for Health Research, the Swartz Foundation, NIH grants
15 R01-EY028723, T32 EY020503-06, T32 MH020002-16A, P30 EY019005, and BrainsCAN at
16 Western University through the Canada First Research Excellence Fund (CFREF). The authors
17 would like to thank Katie Williams, Sean Adams, and Mat LeBlanc, and Tom Franken for their
18 contributions to this project.

19 **Abstract**

20 Populations of cortical neurons generate rhythmic fluctuations in their ongoing spontaneous
21 activity. These fluctuations can be seen in the local field potential (LFP), which reflects
22 summed return currents from synaptic activity in the local population near a recording
23 electrode. The LFP is spectrally broad and many researchers view this breadth as containing
24 many narrowband oscillatory components which may have distinct functional roles. This view is
25 supported by the observation that the phase of narrowband oscillations are often correlated
26 with cortical excitability and can relate to the timing of spiking activity and the fidelity of sensory
27 evoked responses. Accordingly, researchers commonly "tune in" to these channels by
28 narrowband filtering the LFP. Alternatively, neural activity may be fundamentally broadband
29 and composed of transient, non-stationary rhythms that are difficult to approximate as
30 oscillations. In this view, the instantaneous state of the broad ensemble relates directly to the
31 excitability of the local population with no particular allegiance to any frequency band. To test
32 between these alternatives, we asked whether the spiking activity of neocortical neurons in
33 marmoset of either sex is better aligned with the phase of the LFP within narrow frequency
34 bands, or with a broadband measure. We find that the phase of broadband LFP fluctuations
35 provides a better predictor of spike timing than the phase after filtering in narrow bands. These
36 results challenge the view of the neocortex as a system composed of narrow-band oscillators,
37 and supports a view in which neural activity fluctuations are intrinsically broadband.

38 **Significance Statement:** Research into the dynamical state of neural populations often
39 attribute unique significance to the state of narrowband oscillatory components. However,
40 rhythmic fluctuations in cortical activity are non-stationary and broad spectrum. We find that the
41 timing of spontaneous spiking activity is better captured by the state of broadband fluctuations
42 over any latent oscillatory component. These results suggest narrowband interpretations of
43 rhythmic population activity may be limited, and broader representations may provide higher
44 fidelity in describing moment-to-moment fluctuations in cortical activity.

45 **Introduction**

46 Since the first human electroencephalogram (EEG) recordings by Hans Berger(Berger,
47 1929), neuroscientists have inferred cortical function from the state of rhythmic fluctuations in
48 neural population activity(Buzsaki, 2004; Wang, 2010). These brain rhythms are believed to
49 arise from return currents generated by large scale spiking activity in cortical neural
50 populations(Logothetis, 2003; Katzner et al., 2009; Buzsáki et al., 2012). When recorded
51 intracranially with penetrating electrodes, rhythmic activity can be measured in the local field
52 potential (LFP), which typically reflects neural signals arising within ~250 μ M of the electrode
53 tip(Katzner et al., 2009; Lindén et al., 2011). LFP fluctuations are spectrally broad, but are
54 often thought to be composed of activity in narrow frequency bands correlated with distinct
55 neural functions(Canolty et al., 2010; Einevoll et al., 2013; Friston et al., 2015). For example, in
56 the visual cortex, alpha band rhythms (8-15 Hz) are thought to reflect feedback processes of
57 suppression(Jensen and Mazaheri, 2010; van Kerkoerle et al., 2014) and have been shown to
58 be attenuated with or modulated by attention(Worden et al., 2000),(Busch and VanRullen,
59 2010). Beta band rhythms (15-30 Hz) have been linked to motor planning(Sanes and
60 Donoghue, 1993; Rubino et al., 2006) and feedback regulation of excitability(Bastos et al.,
61 2015; Friston et al., 2015). Theta band (4-8 Hz) activity has been related to attention(Fiebelkorn and Kastner, 2019), working memory load(Jensen and Tesche, 2002) and
62 hippocampal function(Buzsáki, 2002). Delta band (< 4 Hz) activity has been related to sleep
63 and states of arousal(Sanes and Donoghue, 1993; Steriade et al., 2001; McGinley et al.,
64 2015). Higher frequency gamma activity (30-90 Hz) has been linked to local coordination in
65 excitation and inhibition(Brunel and Wang, 2003; Bartos et al., 2007; Buzsáki and Wang,
66 2012), attention(Fries et al., 2001, 2008; Gregoriou et al., 2009), memory(Pesaran et al., 2002;
67 Colgin et al., 2009; van Vugt et al., 2010; Lundqvist et al., 2018), and perception(Singer and
68 Gray, 1995; Panagiotaropoulos et al., 2012; Misselhorn et al., 2019), and has been used as a
69 surrogate for measuring cortical activation(Crone et al., 2006; Ray et al., 2008a; Anon, 2013).
70

71 Oscillatory activity can be induced under certain conditions, such as the increased low
72 frequency power that is observed in the EEG when eyes are closed(Berger, 1929; Geller et al.,
73 2014), optogenetically(Lu et al., 2015; Bitzenhofer et al., 2017; Zutshi et al., 2018),
74 electrically(Contreras et al., 1997; Kirov et al., 2009; Escobar Sanabria et al., 2020), or
75 pharmacologically as in the alpha oscillations that occur in medial prefrontal cortex under
76 propofol induced anesthesia(Purdon et al., 2013; Flores et al., 2017; Bastos et al., 2021).

77 It has been proposed that certain frequency bands play a privileged role in routing
78 information among brain areas(Akam and Kullmann, 2010; Bonnefond et al., 2017;
79 Khamechian et al., 2019). The idea that communication between brain areas occurs through
80 oscillatory processes within narrow frequency bands bears similarity to a radio, where signals
81 are broadcast within different frequency bands and a receiver can be tuned to receive
82 them(Hoppensteadt and Izhikevich, 1998). For example, the idea of cross-cortical
83 communication through coherence views synchrony in gamma oscillations as periods of
84 coordination between pre- and postsynaptic groups so as to transmit signals about, for
85 example, an attended stimulus while blocking competing inputs(Fries, 2015). These patterns of
86 gamma-band synchronization are proposed to be regulated across cortical areas by top-down
87 signals within a slower (8-20 Hz) frequency band(Bastos et al., 2015). Other theories posit that
88 the LFP is composed of multiplexed oscillatory neural signals that are separate streams of
89 information processing(Lisman and Idiart, 1995; Panzeri et al., 2010; Akam and Kullmann,
90 2014; Tingley et al., 2018). If oscillatory activity in separate frequencies encodes distinct
91 information channels, and the spiking activity of neurons are the fundamental units of
92 information transmission in the nervous system, then the spiking activity of individual neurons
93 should show preferential alignment of their spiking activity to oscillatory rhythms in order to
94 "tune in" to a channel of information(Canolty et al., 2010; Belluscio et al., 2012). There is
95 evidence to suggest this can occur, as spikes have been found to preferentially align with the

96 phase of theta(Takahashi et al., 2014; Souza and Tort, 2017; Strüber et al., 2022),
97 alpha(Haegens et al., 2011), gamma(Fries et al., 2001; Womelsdorf et al., 2007; Ray et al.,
98 2008b), and beta(Donoghue et al., 1998; Canolty et al., 2010) frequencies.

99 An alternative view is that neurons spike with no preference for any particular
100 narrowband frequency. Rather, spiking is modulated by the instantaneous state of fluctuations
101 in the local population, which varies from moment to moment across a broad range of
102 frequencies. Supporting this view is the observation that balanced excitation and inhibition
103 creates fluctuating neural activity patterns in the awake state, which often exhibit $1/f^{\alpha}$ power
104 spectra across a broad range of frequencies(Destexhe et al., 2001; Gao et al., 2017). Studies
105 in humans have found that changes in cognitive state are associated with broad spectral
106 changes in the EEG(Voytek et al., 2015). The membrane potential of individual neurons is
107 correlated with the population fluctuations measured in the instantaneous LFP(Haider et al.,
108 2016), as opposed to any narrowband component, which suggests the broadband LFP is
109 therefore informative about the instantaneous excitability of neurons in the population(Davis et
110 al., 2020). Accordingly, previous work has found that spikes are weakly coupled to all
111 frequencies of the broadband LFP(Martin and Schröder, 2016), and specific interactions in
112 narrowband frequencies may at times be due to spurious artifacts from narrowband
113 filtering(Scheffer-Teixeira and Tort, 2016).

114 Even when approximately oscillatory activity may be transiently apparent in LFP
115 recordings, it is difficult to describe the phase of neural fluctuations within a narrow range of
116 frequencies because of their non-stationarity(Pesaran et al., 2018). LFP phase is a useful
117 measure for tracking the state of neural fluctuations because it is indicative of the relative
118 transition in the balance of excitation and inhibition with, for example, the falling phase
119 reflecting a transition from inhibition to excitation, and the rising phase transitioning from
120 excitation to inhibition(Atallah and Scanziani, 2009; Poo and Isaacson, 2009; Isaacson and

121 Scanziani, 2011; Teleńczuk et al., 2017). This is in contrast to amplitude measures, which can
122 be ambiguous as the same negative voltage value could reflect neurons becoming more
123 depolarized or more hyperpolarized depending on the signal history. Under this view, one can
124 better characterize the state of neural populations from the phase of broadband fluctuations in
125 LFP activity and neurons will show preferential alignment of their spiking activity to the
126 broadband signal phase, not to any narrowband oscillatory phase.

127 In order to ask whether neuronal spiking is better coupled to narrowband oscillations or
128 broadband fluctuations during waking visual function, we compared spike-phase coupling after
129 filtering the LFP in various filter bands. If the spiking probability of a neuron is phase-locked
130 with the LFP within some frequency band, this is evidence that the neuron in question
131 participates, to some degree, in oscillatory activity of the larger ensemble of neurons whose
132 transmembrane currents give rise to that rhythm. If narrowband rhythms do reflect distinct
133 information channels, then the phase of these oscillations should be particularly informative
134 about the excitability of neurons participating in that oscillatory rhythm, and therefore the timing
135 of their spontaneous spiking activity. Alternatively, if the excitability of the population is
136 reflected in the phase of the broad spectrum fluctuations, then the spiking activity of neurons
137 should be more poorly predicted by any individual oscillatory component and better predicted
138 by the phase of the broadband LFP. Therefore, in this work we take the magnitude of spike-
139 phase coupling as a direct measure of the degree to which oscillatory activity reflects a discrete
140 information channel.

141 The ability to test between these alternatives has been limited, however, because the
142 calculation of phase using the Hilbert Transform breaks down when the frequency content of a
143 signal is too broad(Le Van Quyen et al., 2001). It had been infeasible to directly compare the
144 relative phase-coupling of spiking activity to narrow- or broadband LFP signals without
145 consideration of this potential confound. To overcome this technical limitation, we have

146 developed a measure of phase (Generalized Phase, GP)(Davis et al., 2020), a generalization
147 of the Hilbert Transform that can be applied to spectrally broad signals, allowing us to directly
148 compare narrow- and broadband phase estimates of cortical excitability. This enabled us to
149 test whether the timing of spontaneous spiking activity in cortical populations is better aligned
150 with the phase of classically defined narrowband oscillations, similar to channels on a radio, or
151 is more tightly coupled to the phase of the broad ensemble of non-stationary components. In
152 recordings made from the marmoset middle temporal (MT) extrastriate visual cortex, we find
153 that spontaneous spiking is more strongly phase-coupled to the broadband LFP than to any
154 individual narrow band. Thus, fluctuations in spontaneous neuronal spiking are not coupled
155 preferentially to individual narrowband oscillations, but rather track with the instantaneous
156 fluctuations of neural activity as they change from moment to moment.

157 **Materials and Methods**

158 *Electrophysiology Recordings*

159 One male (monkey W) and one female (monkey T) marmoset monkey (*Callithrix*
160 *jacchus*) was surgically implanted with a headpost for head stabilization and eye tracking. The
161 headpost contained a hollow chamber housing an Omnetics connector for a Utah array
162 (Blackrock Microsystems), which was implanted in a 7x10 mm craniotomy over area MT
163 (stereotaxic coordinates 2 mm anterior, 12 mm dorsal). An 8x8 (64 channel, monkey W) and
164 9x9 with alternating channels removed (40 channel, monkey T) Utah array was chronically
165 implanted over area MT using a pneumatic inserter wand. The electrode spacing was 400 μ M
166 with a pitch depth of 1.5 mm. The craniotomy was closed with Duraseal (Integra Life Sciences,
167 monkey W) or Duragen (Integra Life Sciences, monkey T), and covered with a titanium mesh
168 embedded in dental acrylic. All surgical procedures were performed with the monkeys under
169 general anesthesia in an aseptic environment in compliance with NIH guidelines. All

170 experimental methods were approved by the Institutional Animal Care and Use Committee
171 (IACUC) of the Salk Institute for Biological Studies and conformed with NIH guidelines. Data
172 used in this study was previously used in Davis et al., 2020.

173 Marmosets were trained to enter a custom-built marmoset chair that was placed inside
174 a faraday box with an LCD monitor (ASUS VG248QE) at a distance of 40 cm. The monitor was
175 set to a refresh rate of 100 Hz and gamma corrected with a mean gray luminance of 75
176 candelas/m². Electrode voltages were recorded from the Utah arrays using two Intan RHD2132
177 amplifiers connected to an Intan RHD2000 USB interface board. Data were sampled at 30 kHz
178 from all channels. The marmosets were headfixed by a headpost for all recordings. Eye
179 position was measured with an IScan CCD infrared camera sampling eye position at 500 Hz.
180 Stimulus presentation and behavioral control was managed through MonkeyLogic(Asaad et al.,
181 2013) in Matlab. Digital and analog signals were coordinated through National Instrument DAQ
182 cards (NI PCI6621) and BNC breakout boxes (NI BNC2090A). Neural data was broken into two
183 streams for offline processing of spikes (single-unit and multi-unit activity) and LFPs. Spike
184 data was high-pass filtered at 500 Hz and candidate spike waveforms were defined as
185 exceeding 4 standard deviations of a sliding 1 second window of ongoing voltage fluctuations.
186 Artifacts were rejected if appearing synchronously (within 0.5 ms) on over a quarter of all
187 recorded channels. Segments of data (1.5 ms) around the time of candidate spikes were
188 selected for spike sorting using principal component analysis through the open source spike
189 sorting software MClust in Matlab (A. David Redish, University of Minnesota). Sorted units
190 were classified as single- or multi-units and single units were validated by the presence of a
191 clear refractory period in the autocorrelogram. LFP data was low-pass filtered at 300 Hz and
192 down-sampled to 1000 Hz.

193 *Fixation Behavior*

194 The marmosets were trained to saccade to a marmoset face to initiate each trial. Upon
195 the gaze arriving at the face, it disappeared and was replaced with a white fixation point (0.15
196 DVA). The marmosets held fixation on the fixation point (1.5 visual degree tolerance) for a
197 minimum duration (400 ms monkey W, 300 ms monkey T) awaiting the appearance of a drifting
198 Gabor target (4 DVA diameter; appearing 6-7 DVA eccentricity at 1 of 2 equally eccentric
199 locations in the visual field contralateral to the recording array). Spontaneous data were
200 analyzed from the period of fixation preceding the appearance of a target and excluding the
201 initial 100 ms following fixation initiation. Early fixation breaks (defined by the excursion of the
202 eye position from the fixation window) were excluded from analysis.

203 Free-viewing Natural Scenes

204 Marmosets were headfixed and their gaze monitored as in the previous task. Grayscale
205 versions of naturalistic images (spanning 20-30 DVA) were randomly interleaved and
206 presented to the monkey. The monkey was free to look at the images, and after 10 seconds
207 was given a juice reward. Visual activity was analyzed as in the spontaneous fixation data
208 excluding a 250 msec window around the times of saccades. Saccades were defined as
209 velocity peaks exceeding 25 degrees per second. The time of saccade was taken from the
210 peak velocity after threshold crossing. Velocity was calculated from the absolute value of the
211 first numerical derivative of the smoothed vertical and horizontal eye traces (5 ms sliding
212 Gaussian). We excluded from our analysis spikes that occurred from 50 ms before to 200 ms
213 after detected saccades. Multi-unit spiking activity from two recording sessions in Monkey T
214 and one session in Monkey W (N = 142 units) were combined and analyzed as there was no
215 significant difference in SPI effects between the monkeys ($p = 0.10$; Wilcoxon rank-sum test).

216 *Spike Artifact Elimination*

217 In order to eliminate spike artifacts from the LFP, we applied a de-spiking algorithm first
218 described in Zanos et al. 2011(Zanos et al., 2011). The goal of the algorithm is to eliminate the
219 contribution of spike waveforms to the signal that, after being down-sampled and low-pass
220 filtered, constitutes the LFP. The algorithm assumes the LFP is based on the measured
221 wideband voltage trace recorded from the electrode (y) which is composed of a low-frequency
222 signal (the LFP, w), high-frequency spike components η^k , an offset μ , and white noise ε .

223 Eq. 1:

$$y = w + \sum_{k=1}^m \eta^k + \mu + \varepsilon$$

224 Here, m is the number of spikes for k th neuron k . The high-frequency component of k is the
225 convolution of the spike train s^k and the spike waveform ϕ^k

226 Eq. 2:

$$\eta^k = \phi^k * s^k$$

227
228 Rather than using a spike-triggered average (STA) approach to generate a mean template of
229 the spike waveform which is subtracted at the time of each spike, the algorithm optimally
230 estimates the local field potential w , each spike waveform ϕ^k , and the offset μ which adjusts for
231 the fact that spike waveforms tend to be negative.

232

233 The first assumption is that the LFP is smooth with most of its power in the lower frequencies

234 Eq. 3:

$$p(w) = N(0, \gamma^2 \Gamma)$$

235
236 $N(a, \Sigma)$ represents a multivariate Gaussian with mean a and covariance Σ . Γ is a matrix
237 representing the assumption of smoothness. Multiplying with some vector x (i.e. Γx) produces

238 a low-pass filtered version of x . γ controls the strength of the prior. The second assumption is
 239 that ε is generated by a white noise process $p(\varepsilon) = N(0, 2I)$. The final assumption is that the
 240 spike waveforms ϕ^k lie in a subspace B where $\varphi^k = B\phi^k$ and the spike waveforms are
 241 described in a 1.5 ms interval around the peak depolarization. Bayesian inference was used to
 242 obtain maximum a posteriori (MAP) model parameters for the LFP w , the spike waveforms ϕ^k ,
 243 and the offset μ . By Bayes' theorem, the log-posterior model is
 244 Eq. 4:

$$p(w, \phi^k, \mu | y) \propto p(y|w, \phi^k, \mu) p(w) = k \exp \left[-\frac{1}{2\sigma^2} \sum_i \left(y - w - \sum_{k=1}^m \eta^k - \mu \right)_i^2 - \frac{1}{2\gamma^2} w \Gamma^{-1} w \right]$$

245 where k is a constant factor. The partial derivatives with respect to the parameters are set to 0
 246 and the log of this expression provides the MAP estimates of the parameters \bar{w} , $\bar{\varphi}^k$, and $\bar{\mu}$.
 247 Eq. 5:

$$\begin{aligned} \bar{w} &= (\gamma^2 \Gamma + \sigma^2 I)^{-1} \gamma^2 \Gamma \left[y - \sum_k s^k * (B\bar{\varphi}^k) - \bar{\mu} \right] \\ \bar{\varphi}^k &= (s^k * B) + \left[y - \bar{w} - \sum_{j \neq k} s^j * (B\bar{\varphi}^j) - \bar{\mu} \right] \\ \bar{\mu} &= \frac{1}{n} \sum_k \left[y - \bar{w} - \sum_k s^k * (B\bar{\varphi}^k) \right] \end{aligned}$$

248 An implementation of this algorithm in MATLAB is available from the original authors' website
 249 (<http://apps.mni.mcgill.ca/research/cpack/lfpcode.zip>).

250 *Generalized Phase*

251 We calculated Generalized Phase (GP) as described previously (Davis et al., 2020). The
 252 purpose of GP is to mitigate the breakdown of the analytic signal representation for spectrally
 253 broad signals. As an initial step in the GP representation, then, we filter the signal within a wide
 254 bandpass (i. e. 5-50 Hz; 4th-order zero-phase Butterworth filter), excluding low-frequency

255 content that contributes to origin offsets in the complex plane that distort the estimate of phase
256 angles for higher frequency signals. We then use the single-sided Fourier transform
257 approach(Johansson, 1999; Marple, 1999) on the wideband signal and compute phase
258 derivatives as finite differences, which are calculated by multiplications in the complex
259 plane(Feldman, 2011/4; Muller et al., 2014, 2016). High-frequency intrusions appear in the
260 analytic signal representation as complex riding cycles(Feldman, 2011/4), which manifest as
261 periods of negative frequencies in the analytic signal representation. As a secondary step we
262 then numerically detect these complex riding cycles (N_c points of negative frequency) and
263 utilize shape-preserving piecewise cubic interpolation on the next $2N_c$ points following the
264 detected negative frequency epoch. The resulting representation captures the phase of the
265 largest fluctuation on the recording electrode at any moment in time (Fig. 1f), without the
266 distortions due to the large, low-frequency intrusions or the smaller, high-frequency intrusions
267 characteristic of the $1/f$ -type fluctuations in cortical LFP(Pereda et al., 1998; Linkenkaer-
268 Hansen et al., 2001; Milstein et al., 2009). All phase estimates of filtered LFP segments were
269 calculated using the GP algorithm.

270 *Spike-phase coupling*

271 3 second LFP epochs centered on the period of fixation were analyzed during the
272 fixational behavioral task. The LFP segments were filtered (4th-order zero-phase Butterworth
273 filter with varying filter bandwidths depending on the analysis condition) and spike-phase
274 coupling was calculated over epochs of fixation excluding the initial 100 ms following fixation
275 initiation. The degree of spike-phase coupling was measured as the mean resultant vector
276 length for the LFP phase distribution collected at the time of observed spikes. This measure
277 was calculated using the `circ_r` function in the Circular Statistics Toolbox for Matlab(Berens,
278 2009). The mean resultant vector r of the spike phase distribution is the normalized sum over
279 complex exponentials of the phase angles ϕ

280 Eq. 6:

$$r = \frac{1}{M} \sum_j^N e^{i\phi_j}$$

281 where M is the number of spikes, and the modulus of r ($|r| \in [0, 1]$) represents the degree of
282 spike phase modulation. The closer the value is to 0, the more uniform the phase distribution.
283 The closer the value is to 1, the more concentrated the phases.

284 *Filtered-Raw LFP Signal to Noise Ratio (SNR)*

285 We calculated the signal to noise ratio (SNR) in dB by computing the ratio of the
286 summed squared magnitude of the filtered LFP (in either theta (4-8 Hz), alpha (8-15 Hz), beta
287 (15-30 Hz) low gamma (30-50 Hz) or the wideband (5-50 Hz) filter) to the summed squared
288 magnitude of the broadband 1-100 Hz LFP. The SNR was calculated over a window
289 corresponding to approximately a single cycle of the mean frequency of each filter band (150
290 ms, 75 ms, 50 ms, 25 ms, and 50 ms respectively). The tested window was slid by 1/5th the
291 window width over the entire fixation period. Only spike times that occurred in a window that
292 exceeded -5 dB SNR was included in the SPI calculation for that narrowband filter.

293 *Generalized Linear Model (GLM) Analysis*

294 In order to compare the relative predictive power of spike timing between multiple
295 narrow and a single wideband measure of LFP phase (GP), we tested GLMs trained to predict
296 the likelihood of spiking activity. In particular, both GLMs were trained using LFP phases
297 recorded at points in time when spikes occurred and an equal size sample of LFP phases,
298 selected at random, when no spike occurred. The first model used as predictors the phase at
299 the time of each spike or non-spike for (1) theta (4-8 Hz), alpha (8-15 Hz), beta (15-30 Hz), and
300 low gamma (30-50 Hz) narrowband filtered LFP. The second model used a single predictor: the
301 narrowband beta phase (15-30 Hz), and the third model also used a single predictor: the

302 wideband (4-50 Hz) LFP GP computed on the same training set. In order to linearize the
303 circular phase variables we used the sine and cosine of each phase value as separate
304 predictors(Cremers and Klugkist, 2018), resulting in 8 predictors for the narrowband model and
305 2 predictors for the single narrow and wideband models.

306 Eq. 7:

$$307 Y_i = \kappa_0 + \kappa_1 \sin(\varphi_\theta) + \kappa_2 \cos(\varphi_\theta) + \kappa_3 \sin(\varphi_\alpha) + \kappa_4 \cos(\varphi_\alpha) + \kappa_5 \sin(\varphi_\beta) + \kappa_6 \cos(\varphi_\beta) + \\ 308 \kappa_7 \sin(\varphi_\gamma) + \kappa_8 \cos(\varphi_\gamma)$$

309

310 Single narrowband GLM:

311 Eq. 8:

$$Y_i = \kappa_0 + \kappa_1 \sin(\varphi_\beta) + \kappa_2 \cos(\varphi_\beta)$$

312

313 Single wideband GLM:

314 Eq. 9:

$$Y_i = \kappa_0 + \kappa_1 \sin(\varphi_{WB}) + \kappa_2 \cos(\varphi_{WB})$$

315 Where the model output Y_i for the phases at time sample i is determined by the coefficients on
316 the sine and cosine of the filtered LFP phase. The GLM was fitted using a binominal logit link
317 function to relate changes in the phase predictor variables to the binary output variable at each
318 time sample (spike or no spike). GLMs were fit to half the data in each data set ($N = 20$ across
319 2 monkeys) and the predictor coefficients were tested on the other half of the data. The
320 predictive power of each GLM was evaluated by measuring the area under the curve (AUC) for
321 the receiver-operator characteristic (ROC) curve generated by comparing each model output's
322 true spike hit rate to the spike false alarm rate given the model output.

323 *Simulated spike and LFP generation*

324 In order to generate surrogate spiking and LFP data, we first generated a normal
325 distribution of random frequency values with a mean of 10 Hz and a standard distribution of 1
326 Hz. We then generated a 100 second sinusoidal signal whose frequency drifted with random
327 draws from the frequency distribution. In the case where spikes were generated from the phase
328 of this narrowband signal, we first filtered this signal between 8-15 Hz and used the phase to
329 generate spike times. We also generated a broadband noise signal generated from a Gaussian
330 distribution with mean of 0 and a standard deviation of 1 whose power spectrum followed a 1/f
331 power-law(Kasdin, 1995). In the case where spikes were generated from the phase of the
332 broadband signal, the drifting sinusoidal and pink noise signals were summed in the frequency
333 domain and transformed back into the temporal domain and filtered between 1-100 Hz. The
334 combination of the sinusoidal signal and the noise signal made up our surrogate LFP signal,
335 which was identical between the alternative spike generating conditions.

336 Spike times were generated using a phase-dependent Poisson spike generator. The
337 phase-dependent spiking probability was defined with a circular-linear function across 21
338 phase bins with a 0% spiking probability at 0 rad phases and a 1% spiking probability at $\pm\pi$ rad
339 phases. At each millisecond in time, a random value was drawn from a Poisson distribution
340 whose lambda corresponded to the probability of a spike occurring at the phase of either the
341 sinusoidal (narrowband hypothesis) or surrogate LFP (broadband hypothesis) signal at that
342 millisecond. Any drawn value that exceeded 0 produced a single spike time. The relative
343 phase-dependent spike probabilities produced irregular spike trains with mean firing rates
344 roughly between 5-6 Hz in both conditions. The calculation of spike-phase coupling was
345 performed identically as to that in the recorded data. The surrogate LFP was filtered in either
346 narrow or wide filters and the GP was drawn at the time of each spike to generate spike-phase
347 distributions.

348 *Statistical Analysis*

349 Statistical tests used in this study include the parametric pair-wise student's t test, the
350 non-parametric Wilcoxon signed-rank test, and Wilcoxon rank sum test. Two monkeys were
351 used in this work. No power analyses were performed as the number of monkeys used
352 followed with standard conventions to reduce the number of primates required for neuroscience
353 research. All results were consistent across both monkeys and were therefore collapsed for
354 analysis. Individual measurements within $N = 20$ recording session were averaged and
355 statistical tests were performed on the averages across recording sessions.

356 Author Contributions: Conceptualization, Z.W.D., J.R., L.M.; Data Curation, Z.W.D.; Formal
357 Analysis, Z.W.D.; Funding Acquisition, Z.W.D., J.R.; Investigation, Z.W.D., L.M.; Methodology,
358 Z.W.D., L.M.; Supervision, J.R., L.M.; Visualization, Z.W.D., L.M.; Writing - original draft,
359 Z.W.D., J.R., L.M.; Writing - review and editing, Z.W.D., J.R., L.M.

360 Materials & Correspondence: Correspondence and requests for material should be addressed
361 to J.R and Z.W.D.

362 Data Availability: The data that support the findings of this study are available from the
363 corresponding author upon reasonable request.

364 Code Availability: An open-source code repository for the Generalized Phase algorithm is
365 available on <http://mullerlab.github.io>.

366 **Results**

367 We measured spike-phase coupling for single- and multi-unit spiking activity across
368 traditional narrowband and broadband filtered LFP signals. Spiking activity and LFP data were
369 previously recorded from chronically implanted multielectrode arrays (Utah array, Blackrock
370 Microsystems) in Area MT of two common marmosets (*Callithrix jacchus*; 10 recording
371 sessions in each monkey) as they fixated a point on an otherwise blank screen (gray
372 background, 75 candela/m²; Figure 1a), awaiting the appearance of a faint visual target during
373 a challenging visual detection task(Davis et al., 2020). Similar experimental paradigms have
374 been used to study the relationship between pre-stimulus oscillatory phase and sensory

375 processing and behavioral performance(Busch et al., 2009; Balasubramanian et al., 2020;
376 Zareian et al., 2020). The raw LFP (filtered from 1-100 Hz) sporadically exhibited rhythmic
377 fluctuations across a range of timescales, but there was not a clear peak in the power spectral
378 density that would be consistent with a clear and consistent oscillatory component (Figure 1b).

379 The LFP during periods of fixation was filtered in classically defined frequency bands—
380 theta (4-8 Hz), alpha (8-15 Hz), beta (15-30 Hz), and low gamma (30-50 Hz)—or in a wideband
381 filter that spanned all of these narrow bands from 5-50 Hz (Figure 1c-g). The bounds of the
382 wideband filter were selected to exclude low frequency fluctuations (< 5 Hz) that are
383 associated with slow changes in arousal(Steriade et al., 2001; Petersen et al., 2003), and high
384 frequency components that may be contaminated by spiking artifacts and could, therefore,
385 induce spurious spike-LFP correlations(Ray et al., 2008a; Zanos et al., 2011). However, it
386 could be possible spiking artifacts exist at sub-50 Hz frequencies, which could, in principle,
387 bias our estimate of the relationship between spiking activity and LFP phase in our broadband
388 representation. To mitigate this potential confound, we performed a “de-spiking” procedure on
389 the data as described in Zanos et al. 2011(Zanos et al., 2011). This removes spike waveforms
390 from the raw (30 KHz) recorded electrode data signals through spike-waveform subtraction and
391 interpolation before downsampling and filtering into the LFP. Any remaining relationship
392 between the phases of sub-50 Hz activity in any frequency band must therefore be due to an
393 indirect relationship between the population currents that give rise to the LFP and individual
394 neuronal spiking, and not the direct contribution of that spike occurring itself.

395 If spiking activity is either organized into oscillations, giving rise to narrowband
396 fluctuations in the LFP, or if LFP oscillations reflect population-wide subthreshold fluctuations
397 that modulate the probability of spiking within a particular band, then spikes should tend to be
398 aligned in phase with the LFP, within these frequency ranges. Alternatively, if no individual
399 rhythmic component of the LFP dictates the excitability of neurons, but rather the precise,

400 moment-by-moment fluctuations of the LFP reflect the state of the population, we would expect
401 spikes to occur more often at phases of the broadband LFP that correspond to states of
402 depolarization across the local population, regardless of frequency.

403 To test these competing hypotheses, we measured the phase of each filtered LFP
404 signal at the times of multi-unit spiking activity. Phase is conventionally measured for
405 oscillatory or spectrally narrow signals by calculating the analytic signal(Feldman, 2011/4;
406 Marple, 1999), where instantaneous amplitude and phase can be expressed in polar
407 coordinates and whose real and imaginary parts are related to each other by the Hilbert
408 Transform. However, for spectrally broad signals, the standard computational implementations
409 break down(Le Van Quyen et al., 2001). Low frequencies can shift the analytic signal
410 representation by a constant in the complex plane, distorting the estimated phase angle. In
411 addition, high frequency intrusions introduce complex riding cycles that generate phase
412 reversals and appear as negative frequencies which distort the analytic signal. To address
413 these problems, we introduced an updated approach to the analytic signal representation,
414 termed “generalized phase” (GP)(Davis et al., 2020). Briefly, in this approach we first impose a
415 high-pass cutoff on the signal (5 Hz). This step aims to eliminate low-frequency intrusions,
416 while also preserving a significant portion of the signal spectrum and minimizing waveform
417 distortion. Second, we identify negative frequencies, which can arise from high-frequency
418 intrusions, and remove them, replacing the phase values with shape-preserving interpolation.
419 This approximates the continuation of the dominant fluctuation’s trajectory. The result, after
420 filtering, is an estimate of phase that tracks with the dominant frequency component of the LFP
421 as it shifts over time (Figure 2a) while minimizing phase distortions that arise due to
422 narrowband filtering a non-stationary broad spectrum signal such as the raw LFP(Yael et al.,
423 2018). All results reported here, for both broadband and narrowband filtered data, were
424 computed using GP. Low- and high-frequency intrusions are rare in narrowband filtered signals

425 so, for narrowband filtered data, computation of GP should yield very similar phase estimates
426 to those estimated using the Hilbert transform. To confirm this, all analyses were repeated for
427 narrowband filtered signals using the Hilbert Transform. As expected, the results were virtually
428 identical. All future mentions of phase therefore refer to the GP of the signal.

429 The phase of the wideband filtered signal is strongly coupled to the timing of measured
430 multi-unit spiking activity (Figure 2b). We measured an index of the coupling of spikes to each
431 filtered LFP by calculating the mean resultant length of the circular spike-phase distribution.
432 This spike-phase coupling index (SPI) value ranges from 0 (uniform spike-phase distribution) to
433 1 (spikes perfectly coupled to a single phase), and for the 5-50 Hz wideband filtered signal, the
434 average SPI was 0.15 ± 0.009 S.E.M. ($N = 20$ sessions across 2 monkeys). The wideband
435 filtered SPI was significantly stronger than the coupling observed after filtering in theta (SPI =
436 0.08 ± 0.005 ; $p < 1 \times 10^{-9}$; two-tailed paired sample t-test), alpha (SPI = 0.07 ± 0.005 ; $p < 1 \times 10^{-10}$),
437 beta (SPI = 0.11 ± 0.007 ; $p < 1 \times 10^{-11}$) or gamma (SPI = 0.08 ± 0.009 ; $p < 1 \times 10^{-9}$) frequency
438 bands (Figure 2c-f). These results suggest that the instantaneous rhythmic state of neuronal
439 excitability is better reflected in the phase of the ensemble LFP activity rather than in the phase
440 of any particular narrowband subcomponent.

441 If oscillations reflect information streams analogous to channels on a radio, then it could
442 be the case that some neurons are more coupled to one embedded oscillation and other
443 neurons are more coupled to a different oscillation, and that by collapsing across multiunit
444 activity the phase-dependence of the spiking activity is diluted for each narrowband filter. If
445 true, we might find stronger spike-phase coupling for the wideband filter across the populations
446 even though individual neurons are best coupled to different narrowband oscillations. To test
447 this, we measured the spike-phase coupling across filters for well-isolated single units in our
448 recordings. We did not find any evidence of differential preference across neurons for
449 narrowband signals. Rather, the majority of neurons had a stronger SPI to the state of the

450 wideband signal as compared to theta (78.50%, N = 107 single units; Figure 3a), alpha
451 (78.50%, Figure 3b), beta (83.18%, Figure 3c), or gamma (85.98%, Figure 3c) filtered signals.
452 Additionally, for the minority of neurons that did show stronger SPI to a narrowband filtered
453 signal, they were more weakly coupled in general (average SPI = 0.09) and did not show
454 specific preference to any one narrowband frequency. Thus, variable population phase-
455 coupling to narrowband signals could not explain why the wideband filtered signals exhibit
456 stronger spike-phase coupling.

457 One possibility is that spike timing is only governed by each narrowband oscillation
458 when that oscillation is strongly present in the data, and as each oscillation is only transiently
459 present, it is unfair to expect, for example, gamma to predict spike timing when gamma is not
460 present in the data. To test this we restricted our analysis to only count spikes for each
461 frequency band at times when there is strong oscillatory power in that band. To do this we
462 calculated the signal-to-noise (SNR) ratio between the filtered and raw (1-100 Hz) LFP and
463 identified epochs where the narrowband signal exceeded a -5 dB threshold for at least 1 cycle
464 of the center frequency of the filter bandwidth. Only spikes that occurred during these epochs
465 were included for that narrowband's SPI measure. Despite restricting each filter band to spikes
466 that occur when those oscillations are transiently apparent in the data, the wideband measure
467 still captures the strongest SPI values (Figure 4a; wideband mean SPI = 0.16 ± 0.010 S. E. M.
468 as compared to theta: 0.11 ± 0.010 , alpha: 0.08 ± 0.005 , beta: 0.12 ± 0.010 , and gamma: 0.09
469 ± 0.005 ; $p < 0.001$, Wilcoxon signed-rank test), while also describing a majority of the recorded
470 data (approximate fraction above dB threshold; wideband: 92% vs. theta: 16%, alpha: 46%,
471 beta: 42%, and low gamma: 19%).

472 Thus, spike timing is better predicted by broadband phase than narrowband phase for
473 any of the bands tested. We next asked how well spike timing could be predicted based on the
474 combination of all four narrowband filtered signals. To test this we constructed a generalized

475 linear model (GLM) that took as its input the phase values measured over the four narrow band
476 frequencies (spanning 4 to 50 Hz) at times when a spike occurred and an equal number of
477 randomly drawn times when no spike occurred. The GLM was trained to predict whether or not
478 a spike occurred, based on the four phases. The model was trained on half the data in each
479 recording session, with the remaining data held out as a test set. The model's ability to predict
480 spiking was measured using Receiver Operator Characteristic (ROC) analysis.

481 We reasoned that if oscillatory activity across the multiple narrow bands drives spiking
482 activity, the four-factor GLM, which has simultaneous access to the phases of all four
483 oscillatory signals, should predict spiking better than a GLM trained to predict spiking based on
484 the phase computed in an individual band (four-factor GLM AUC = 0.578 ± 0.004 S. E. M.;
485 single narrowband GLM AUC = 0.545 ± 0.003 S. E. M.; $p = 0.00009$. Wilcoxon signed-rank
486 test). This analysis shows that more information about spiking is present across multiple
487 bands. This is consistent with two different hypotheses. The first is that the narrow bands
488 capture the individual contribution of oscillations that fall within each band, and the four factor
489 GLM reflects the joint contributions of these oscillatory drivers. An alternative hypothesis is that
490 the processes that drive spiking activity fluctuate over time in their power spectrum, and spiking
491 activity follows these fluctuations over time, regardless of where they travel in frequency. If the
492 first hypothesis is true, the four-factor GLM, which has access to the phase within each band,
493 should perform better than a single-factor broadband GLM, which is provided with a single
494 measure of phase that is blind to the interactions across the same frequency space. If the
495 second hypothesis is true, the single-factor broadband GLM, which uses a measure of phase
496 that tracks with the dominant LFP frequency as it changes over time, should do as well as the
497 four-factor GLM.

498 To test this, a GLM was trained on the same data that was used to train the four-factor
499 GLM, but instead of providing it with four phases computed within the four narrow bands, it was

500 trained using only a unitary measure of phase – GP applied to the wideband (4-50 Hz) signal
501 as its input, and its ability to predict spiking was measured using the same ROC analysis. As
502 shown in Figure 4b, there was no significant difference in the ability of the combined 4
503 narrowband or one wideband GLM to predict spike times as defined by the area under the
504 curve for each session's ROC (wideband mean AUC = 0.579 ± 0.005 S. E. M.; $p = 0.16$,
505 Wilcoxon signed-rank test). Thus, even when combining signals across multiple frequency
506 bands, narrowband filtering adds no information beyond what is already present in the phase of
507 the momentarily dominant fluctuation in the LFP preserved in the wideband representation and
508 as measured using generalized phase.

509 Our results suggest spontaneous neuronal spiking in the neocortex is not organized by
510 oscillatory activity, but rather is modulated by fluctuations in synaptic activity that can be
511 estimated from the instantaneous phase of the broadband LFP. If true, then SPI values should
512 be correlated with how much filtering alters the LFP phase relative to the raw recorded LFP. To
513 test this, we compared the strength of spike-phase coupling to each band pass filtered signal
514 with the degree of correlation between the LFP signal before and after filtering (Figure 4c).
515 There was a significant positive correlation between SPI and the raw-filtered LFP correlation
516 across recording sessions ((Pearson's $r = 0.65 \pm 0.11$ 95% CI, $p < 1 \times 10^{-12}$), suggesting a direct
517 relationship between spike-phase coupling and how well the filtered LFP tracked with the raw
518 LFP.

519 If spikes are more coupled to the broadband LFP than any embedded narrowband
520 oscillation, then the optimal filter band for maximizing SPI should be one that is as broad as
521 possible. To test for an optimal filter band, we scanned across a large parameter space varying
522 the lower and upper bounds of the band pass filter. The lower bound ranged from 1 to 50 Hz
523 and the upper bound ranged from 5 to 125 Hz with a minimum bandwidth of 4 Hz. Consistent
524 with our prior results, the strongest spike-phase coupling was observed for filters that included

525 the largest width of the signal spectrum, with an exception for the lowest frequencies (Figure
526 4d). These results indicate optimal filters for maximizing spike-phase coupling estimates span
527 from 3 Hz in the lower band and as high as we sampled in the upper band (125 Hz), assuming
528 spike-artifacts are effectively removed from high frequency components in the LFP. If not, a
529 cautious step then is maintaining a low-pass filter which serves to help mitigate spurious
530 coupling values due to residual spike artifacts in higher frequencies.

531 Spiking activity can bleed into the LFP, artifactually inflating estimates of spike-phase
532 coupling in high frequency bands. Spike artifacts may be responsible for some gamma phase
533 relationships with spiking activity, as the contribution of spike artifacts in the LFP had been
534 previously observed down to 50 Hz(Ray and Maunsell, 2011; Zanos et al., 2011). To avoid this
535 we performed a de-spiking procedure, and examined the consequence of that de-spiking on
536 SPI estimates. A comparison of SPI values on the same data with and without de-spiking found
537 that the de-spiking procedure significantly reduced SPI values for frequency bands that
538 included frequencies below 50 Hz (but not below 15 Hz) such as low gamma (30-50Hz; not de-
539 spiked SPI = 0.13, $p = 1.65 \times 10^{-7}$ two-tailed Wilcoxon ranked sum test), beta (15-30 Hz; SPI =
540 0.13, $p = 0.026$) and the wideband (5-50 Hz; SPI = 0.18, $p = 0.009$). There was no significant
541 reduction in either alpha (8-15 Hz; SPI = 0.08, $p = 0.067$) or theta (4-8 Hz; SPI = 0.09, $p =$
542 0.190) when we de-spiked the LFP. These observations are consistent with recent reports of
543 spike-artifacts impacting spike-LFP synchronization at frequencies as low as 20 Hz(Banaie
544 Boroujeni et al., 2020). These results argue either that the artificial coupling of spiking activity
545 to LFP phase may be present at low frequencies, or that de-spiking techniques are overly
546 liberal in the removal of spike waveforms. Regardless, even if we consider the possibility that
547 the de-spiking procedure is introducing more noise than it is eliminating, the main result—that
548 the broadband LFP phase produces the strongest SPI values—holds when this technique is
549 not applied and the raw data is left intact.

550 The results described so far are limited to spontaneous activity recorded during a
551 period in which animals fixated a fixation point at the center of a blank screen while awaiting
552 the appearance of a faint visual target. Do these findings generalize to more naturalistic
553 viewing conditions? To test this, we calculated SPI for each frequency band in animals as they
554 freely viewed natural scene images. Since the focus here is on intrinsic fluctuations, not the
555 transient responses that are evoked at the time of the saccade, neural activity at the time of the
556 saccade (from 50 ms before and ending 200 ms after saccades) was eliminated from
557 analysis. Consistent with the pattern observed during fixation of a blank screen, the wideband
558 filtered signal produced the strongest SPI values (0.16 ± 0.008 ; $N = 142$ multi-units across 2
559 sessions in Monkey T and 1 session in Monkey W), which was significantly stronger than the
560 SPI values measured for theta (0.14 ± 0.007 ; $p < 1 \times 10^{-7}$ Wilcoxon signed rank test), alpha
561 (0.13 ± 0.007 ; $p < 1 \times 10^{-16}$), beta (0.10 ± 0.006 ; $p < 1 \times 10^{-14}$), and low gamma (0.11 ± 0.006 ; $p <$
562 1×10^{-12}). Thus the spontaneous coupling of spiking activity to broadband fluctuations is not
563 limited to fixating a blank screen, but is apparent during more dynamic active vision.

564 While our experimental results suggest spiking activity is better correlated with the
565 instantaneous state of the broadband LFP rather than any individual oscillatory component, the
566 ground truth mechanism relating spiking to rhythmic LFP activity is unknown in our recordings.
567 To explore whether our observations can be explained by the hypothesis that spiking activity is
568 coupled to broadband LFP phase as opposed to a narrowband oscillation, we simulated an
569 LFP signal by combining a narrowband oscillatory fluctuation that consisted of spectral power
570 drifting between 8-15 Hz with broad spectrum noise. The power spectral density of this
571 simulated LFP fluctuation was designed to be consistent with the typical 1/f power-law
572 observed in cortical recordings *in vivo* (Miller *et al.*, 2009) (Figure 5d). We then generated spike
573 times from a Poisson spike generator where the probability was dependent on either the phase
574 of the narrowband 8-15 Hz oscillatory signal (hypothesis A; Figure 5a) or the phase of the

575 combined narrowband and broad spectrum signals (hypothesis B; Figure 5b). Spike probability
576 was phase dependent with spikes most likely to occur near $\pm\pi$ radians and spikes least likely
577 to occur near 0 radians. Importantly, the spectral content of the simulated LFP was identical
578 between the two alternative hypotheses and only the timing of spikes differed between the two
579 conditions (Figure 5c).

580 In order to recover the signal correlated with spike-generation we filtered the simulated
581 LFP in either a narrow bandpass filter from 8-15 Hz, or a wide band pass filter from 5-100 Hz.
582 In the case where spikes were correlated with the phase of the narrowband oscillatory
583 component (hypothesis A, blue), the narrowband filtered LFP signal was relatively weakly
584 correlated with the raw simulated LFP (Pearson's $r = 0.49$, Figure 6a). However, spike timing
585 was strongly coupled to the phase of the narrowband filtered LFP signal ($SPI = 0.34 \pm 0.002$
586 S.E.M; $N = 20$ simulations). This coupling was significantly stronger than when using the
587 wideband filter to recover spike phases ($SPI = 0.16 \pm 0.002$ S.E.M; $p = < 0.0001$ two-tailed
588 Wilcoxon signed-rank test; Figure 6b). In the case where the spikes were generated from the
589 phase of the broad spectral content of the simulated LFP (hypothesis B, orange), the wideband
590 filtered LFP was strongly correlated with the raw simulated LFP (Pearson's $r = 0.84$, Figure 6c)
591 and the spike-phase relationship was significantly stronger after filtering in the wideband ($SPI =$
592 0.29 ± 0.002 S.E.M.) as compared to the spike-phase coupling to the narrowband filtered LFP
593 ($SPI = 0.14 \pm 0.002$ S.E.M.; $p = < 0.0001$ two-tailed Wilcoxon signed-rank test; Figure 6d).
594 These results indicate that, in principle, if neurons were coupled to an oscillatory component,
595 then narrowband filtering to extract that oscillation would indeed yield stronger spike-phase
596 coupling than the broadband signal.

597 We next asked whether a narrowband or broadband spike-correlated signal could
598 reproduce the observed relationship of increasing spike-phase coupling with increasing
599 correlation between the filtered and raw LFP signal. We filtered the signal under various filters

600 (theta (4-8 Hz), alpha (8-15 Hz), beta (15-30 Hz), wideband (5-50 Hz)) as in the cortical
601 recordings, as well as a broad band pass from 1-100 Hz, and measured both the spike-phase
602 coupling for narrowband and broadband correlated spike generation and the correlation
603 between the filtered and raw LFP signal. In the case where spikes were correlated with the
604 narrowband signal, the best filter was the 8-15 Hz filter (matching the source of the spike
605 generating signal), followed by the wideband and broadband filters which each included the
606 spike generating signal band within its bandwidth, but also included a smaller and larger part of
607 the “noise” spectrum respectively (Figure 7a). In the case where spikes were correlated with
608 the broadband signal, the best filter was the broadband filter, and decreased as the filters
609 became narrower (Figure 7b). The narrowband spike source had a weak correlation between
610 the SPI (Pearson’s $r = 0.27$), and the degree of filter-raw signal similarity as the optimal filter
611 was one that eliminated the broadband noise from the simulated LFP. In contrast, the
612 broadband spike source reproduced the strong positive correlation between SPI and filtered-
613 raw LFP similarity observed in our recordings (Pearson’s $r = 0.92$; Figure 7c). Our results
614 indicate a model where spikes are coupled to the state of fluctuations in the broad spectral
615 content of the LFP is sufficient to account for our observations *in vivo*, and suggest neuronal
616 spiking is not preferentially coupled to narrowband oscillations.

617 **Discussion**

618 A central goal of systems neuroscience is to understand how brain activity underlies
619 information processing and behavior. Ideally, we would like to record every action potential of
620 every neuron and ask how they relate to one another in the service of behavior, but even with
621 the best available neurophysiological tools -- sets of electrode arrays with contacts numbering
622 in the thousands -- we can only sample a tiny fraction of the neurons in the brain. Therefore,
623 neurophysiologists typically rely on indirect measures of the activity to estimate the spiking
624 statistics of larger cortical populations. These include LFP, EEG, or MEG, which provide
625 indirect measures of the activity of larger populations of neurons. Rhythmic patterns of activity

626 are often observed in these measures, and it is common to treat these rhythmic patterns as
627 meaningful computational units, potentially serving as independent channels of information
628 processing, or if not independent in the context of cross-frequency phase-amplitude
629 coupling(Munia and Aviyente, 2019), at least functionally dissociable from the signal in which
630 they are embedded(Thut et al., 2012; Einevoll et al., 2013), similar to turning the dial on a radio
631 to receive different streams of information.

632 One way of thinking about rhythmic dynamics is that the spiking probabilities of the
633 neurons in the larger population co-vary within some frequency band and that this results in an
634 oscillation — for the example studied here, in the LFP. If so, then by filtering the LFP within that
635 oscillatory band and asking how it relates to some measure of either behavior (e.g.
636 performance on a discrimination task), a neural property (such as spike timing or transmission
637 of information across areas), or its covariation with some behavioral manipulation (e.g.
638 directing attention into or away from the retinotopic locus of the electrode), one can identify the
639 contribution of the oscillation to neural computations or behavior. However there are some
640 problems with treating neural fluctuations as oscillations. First, neural fluctuations are often
641 only transiently rhythmic in the awake state(Jones, 2016), and even then they are not purely
642 sinusoidal(Cole and Voytek, 2017) as they drift in frequency content from moment to moment
643 with changes in arousal(Vinck et al., 2015), attention(Fries et al., 2001), or sensory
644 input(Henrie and Shapley, 2005). Even in the case when neural fluctuations are strongly
645 rhythmic, we find narrowband filtering captures less of the spike-phase relationship than when
646 maintaining a wideband representation. This may be because the application of narrowband
647 filters to signals that are non-stationary in their frequency content can result in a loss of timing
648 precision in phase estimates(Yael et al., 2018).

649 The results presented here argue that neurons are not specifically coupled to
650 narrowband oscillatory activity, but rather it is the state of the broadband moment-to-moment

651 fluctuations that are informative of the relative excitability of the local population. This is not to
652 say that rhythms are not apparent in fluctuating dynamics or that they are irrelevant for cortical
653 function. Nor are we suggesting that rhythmic power is limited to what one would expect from
654 stochastic synchronizations in a 1/f noise process. For example, it is not the case that
655 oscillatory rhythms are only as informative as their fraction of the spectral content of broadband
656 fluctuations. We observed that low gamma filtered signals had stronger SPI values than one
657 might expect based on their relative power in the PSD and given how poorly correlated the
658 gamma filtered signals were to the raw LFP. Similarly, the alpha band filtered signals had much
659 more power and were relatively well correlated with the raw LFP, yet had weaker SPI values
660 than the beta band filtered signals, which were more poorly correlated with the raw LFP.
661 Indeed, there is variation in the degree to which spikes couple to LFP phase across the five
662 frequency bands studied here. However, that does not imply those frequency bands are
663 independent information channels, distinct from the rest of the LFP. It is evident that they are
664 not, as we see the strongest SPI values for the broadest frequency bands.

665 In order to test what one would expect to see if it were the case spikes preferentially
666 coupled to a narrow set of frequencies, we simulated spike trains generated from the phase of
667 oscillatory signals embedded in an otherwise 1/f noise spectrum (Hypothesis A). Under these
668 conditions, we found stronger SPI to the narrowband filter that best matched the signal
669 underlying spike generation signal. We also found a reduction in SPI values when the
670 broadband filter was used. This matches what one would intuitively expect from a system
671 composed of an oscillatory signal combined additively with a broad noise. This is the intuition
672 that often underlies narrowband filtering approaches in electrophysiological signal analysis.
673 While there may be alternative explanations for why a broadband signal produces stronger SPI
674 values in our cortical recordings, the second model, where spikes are fluctuation driven

675 (Hypothesis B), was sufficient to account for the spike-LFP coupling relationships observed in
676 the data.

677 Since the phase of narrowband oscillatory activity does not predict spiking activity as
678 well as the phase of wideband activity, it raises a question as to whether and when narrowband
679 filtering is appropriate to study rhythmic spiking dynamics. The use of narrowband filters
680 assumes a frequency resolved signal in the brain that is embedded in noise. As shown by
681 hypothesis A and in Figure 5, when neural activity is strongly coupled to latent oscillatory
682 activity, narrowband filtering is effective at recovering the signal. Therefore, in situations with
683 steady, ongoing oscillatory activity that has low variance in frequency, such as sleep spindles,
684 hippocampal theta, or gamma oscillations due to strong feed-forward input, narrowband
685 filtering may better capture spiking. However, if the signal is not known, narrowband filtering
686 imposes an assumption of what is signal and noise that may not be warranted and may yield
687 misleading results. Analytic techniques that allow for the contribution of broader frequency
688 ranges, as used here, may reveal the degree to which results are frequency dependent or filter
689 dependent.

690 It is important to note the limitations of the present findings. First, all analyses here
691 have focused on spontaneous activity. We cannot generalize the present results to neural data
692 collected under other conditions such as data collected during stimulus-evoked responses.
693 Some narrow-band frequency ranges, such as the gamma band, do not exhibit much power in
694 the absence of strong sensory input(Henrie and Shapley, 2005; Ray and Maunsell, 2010).
695 Additional experiments will be needed to determine the degree to which gamma band and
696 generalized phase predict spike timing under these conditions. Further, the majority of the data
697 analyzed here were recorded from the visual cortex in monkeys performing a particular task, in
698 which they fixated a fixation spot at the center of a blank screen, awaiting the appearance of
699 a faint visual target. In our spontaneous cortical recordings, which are largely representative of

700 the aperiodic 1/f power law observed in primate visual cortex(Fries et al., 2001; Henrie and
701 Shapley, 2005; Yu and Ferster, 2010), even when oscillations are transiently present,
702 narrowband filtering produces a weaker estimate of the spike-LFP relationship than a wider
703 representation.

704 The Generalized Phase approach used here provides a meaningful measure of phase
705 for spectrally broad signals(Davis et al., 2020), and reveals a stronger relationship between
706 broadband LFP fluctuations and spiking probability than could be estimated from any individual
707 narrowband filtered signal. The advantage of GP over narrowband signals is that it follows the
708 moment-to-moment fluctuations in the signal and provides a phase value that generalizes
709 across changes in frequency content. This approach can reveal patterns that would not be
710 clear from an analysis of narrowband oscillations. For example, analysis of broadband
711 measures of phase led to the discovery that the alignment of spontaneous traveling waves of
712 cortical activity with the retinotopic locations of faint visual targets was predictive of the
713 magnitude of evoked activity and perceptual sensitivity(Davis et al., 2020). These effects were
714 only apparent in the data when the state of broadband LFP fluctuations was considered. When
715 filtered in narrow bands, the predictive power of wave phase on behavioral performance was
716 abolished. Consistent with those findings, the results presented here show that, at least in the
717 spontaneous waking activity of Area MT, the instantaneous state of cortical populations is
718 better estimated from the GP of broadband LFP fluctuations than from any narrowband
719 oscillatory component. These results suggest that the phase of broadband neural fluctuations,
720 rather than any specific narrowband frequency content, is the main influence on spontaneous
721 spiking activity in the cortex.

722 **References**

723 Akam T, Kullmann DM (2010) Oscillations and filtering networks support flexible routing of
724 information. *Neuron* 67:308–320.

725 Akam T, Kullmann DM (2014) Oscillatory multiplexing of population codes for selective
726 communication in the mammalian brain. *Nat Rev Neurosci* 15:111–122.

727 Anon (2013) Cortical gamma oscillations: the functional key is activation, not cognition.
728 *Neurosci Biobehav Rev* 37:401–417.

729 Asaad WF, Santhanam N, McClellan S, Freedman DJ (2013) High-performance execution of
730 psychophysical tasks with complex visual stimuli in MATLAB. *J Neurophysiol* 109:249–260.

731 Atallah BV, Scanziani M (2009) Instantaneous modulation of gamma oscillation frequency by
732 balancing excitation with inhibition. *Neuron* 62:566–577.

733 Balasubramanian K, Papadourakis V, Liang W, Takahashi K, Best MD, Suminski AJ,
734 Hatsopoulos NG (2020) Propagating Motor Cortical Dynamics Facilitate Movement
735 Initiation. *Neuron* 106:526–536.e4.

736 Banaie Boroujeni K, Tiesinga P, Womelsdorf T (2020) Adaptive spike-artifact removal from local
737 field potentials uncovers prominent beta and gamma band neuronal synchronization. *J
738 Neurosci Methods* 330:108485.

739 Bartos M, Vida I, Jonas P (2007) Synaptic mechanisms of synchronized gamma oscillations in
740 inhibitory interneuron networks. *Nature Reviews Neuroscience* 8:45–56 Available at:
741 <http://dx.doi.org/10.1038/nrn2044>.

742 Bastos AM, Donoghue JA, Brincat SL, Mahnke M, Yanar J, Correa J, Waite AS, Lundqvist M,
743 Roy J, Brown EN, Miller EK (2021) Neural effects of propofol-induced unconsciousness

744 and its reversal using thalamic stimulation. *Elife* 10 Available at:
745 <http://dx.doi.org/10.7554/eLife.60824>.

746 Bastos AM, Vezoli J, Bosman CA, Schoffelen J-M, Oostenveld R, Dowdall JR, De Weerd P,
747 Kennedy H, Fries P (2015) Visual areas exert feedforward and feedback influences through
748 distinct frequency channels. *Neuron* 85:390–401.

749 Belluscio MA, Mizuseki K, Schmidt R, Kempter R, Buzsáki G (2012) Cross-frequency phase-
750 phase coupling between θ and γ oscillations in the hippocampus. *J Neurosci* 32:423–435.

751 Berens P (2009) CircStat: MATLABToolbox for Circular Statistics. *Journal of Statistical
752 Software* 31 Available at: <http://dx.doi.org/10.18637/jss.v031.i10>.

753 Berger H (1929) Über das Elektrenkephalogramm des Menschen. *Archiv für Psychiatrie und
754 Nervenkrankheiten* 87:527–570 Available at: <http://dx.doi.org/10.1007/bf01797193>.

755 Bitzenhofer SH, Ahlbeck J, Wolff A, Simon Wiegert J, Gee CE, Oertner TG, Hanganu-Opatz IL
756 (2017) Layer-specific optogenetic activation of pyramidal neurons causes beta-gamma
757 entrainment of neonatal networks. *Nature Communications* 8 Available at:
758 <http://dx.doi.org/10.1038/ncomms14563>.

759 Bonnefond M, Kastner S, Jensen O (2017) Communication between Brain Areas Based on
760 Nested Oscillations. *eNeuro* 4 Available at: <http://dx.doi.org/10.1523/ENEURO.0153-16.2017>.

762 Brunel N, Wang X-J (2003) What Determines the Frequency of Fast Network Oscillations With
763 Irregular Neural Discharges? I. Synaptic Dynamics and Excitation-Inhibition Balance.
764 *Journal of Neurophysiology* 90:415–430 Available at:
765 <http://dx.doi.org/10.1152/jn.01095.2002>.

766 Busch NA, Dubois J, VanRullen R (2009) The phase of ongoing EEG oscillations predicts visual
767 perception. *J Neurosci* 29:7869–7876.

768 Busch NA, VanRullen R (2010) Spontaneous EEG oscillations reveal periodic sampling of
769 visual attention. *Proc Natl Acad Sci U S A* 107:16048–16053.

770 Buzsáki G (2002) Theta Oscillations in the Hippocampus. *Neuron* 33:325–340 Available at:
771 [http://dx.doi.org/10.1016/s0896-6273\(02\)00586-x](http://dx.doi.org/10.1016/s0896-6273(02)00586-x).

772 Buzsaki G (2004) Neuronal Oscillations in Cortical Networks. *Science* 304:1926–1929 Available
773 at: <http://dx.doi.org/10.1126/science.1099745>.

774 Buzsáki G, Anastassiou CA, Koch C (2012) The origin of extracellular fields and currents —
775 EEG, ECoG, LFP and spikes. *Nature Reviews Neuroscience* 13:407–420 Available at:
776 <http://dx.doi.org/10.1038/nrn3241>.

777 Buzsáki G, Wang X-J (2012) Mechanisms of gamma oscillations. *Annu Rev Neurosci* 35:203–
778 225.

779 Canolty RT, Ganguly K, Kennerley SW, Cadieu CF, Koepsell K, Wallis JD, Carmen JM (2010)
780 Oscillatory phase coupling coordinates anatomically dispersed functional cell assemblies.
781 *Proc Natl Acad Sci U S A* 107:17356–17361.

782 Cole SR, Voytek B (2017) Brain Oscillations and the Importance of Waveform Shape. *Trends
783 Cogn Sci* 21:137–149.

784 Colgin LL, Denninger T, Fyhn M, Hafting T, Bonnevie T, Jensen O, Moser M-B, Moser EI (2009)
785 Frequency of gamma oscillations routes flow of information in the hippocampus. *Nature*
786 462:353–357.

787 Contreras D, Destexhe A, Sejnowski TJ, Steriade M (1997) Spatiotemporal patterns of spindle
788 oscillations in cortex and thalamus. *J Neurosci* 17:1179–1196.

789 Cremers J, Klugkist I (2018) One Direction? A Tutorial for Circular Data Analysis Using R With
790 Examples in Cognitive Psychology. *Front Psychol* 9:2040.

791 Crone NE, Sinai A, Korzeniewska A (2006) High-frequency gamma oscillations and human
792 brain mapping with electrocorticography. *Prog Brain Res* 159:275–295.

793 Davis ZW, Muller L, Martinez-Trujillo J, Sejnowski T, Reynolds JH (2020) Spontaneous
794 travelling cortical waves gate perception in behaving primates. *Nature* 587:432–436.

795 Destexhe A, Rudolph M, Fellous JM, Sejnowski TJ (2001) Fluctuating synaptic conductances
796 recreate in vivo-like activity in neocortical neurons. *Neuroscience* 107:13–24.

797 Donoghue JP, Sanes JN, Hatsopoulos NG, Gaál G (1998) Neural discharge and local field
798 potential oscillations in primate motor cortex during voluntary movements. *J Neurophysiol*
799 79:159–173.

800 Einevoll GT, Kayser C, Logothetis NK, Panzeri S (2013) Modelling and analysis of local field
801 potentials for studying the function of cortical circuits. *Nature Reviews Neuroscience*
802 14:770–785 Available at: <http://dx.doi.org/10.1038/nrn3599>.

803 Escobar Sanabria D, Johnson LA, Yu Y, Busby Z, Nebeck S, Zhang J, Harel N, Johnson MD,
804 Molnar GF, Vitek JL (2020) Real-time suppression and amplification of frequency-specific
805 neural activity using stimulation evoked oscillations. *Brain Stimul* 13:1732–1742.

806 Feldman M (2011/4) Hilbert transform in vibration analysis. *Mech Syst Signal Process* 25:735–
807 802.

808 Fiebelkorn IC, Kastner S (2019) A Rhythmic Theory of Attention. *Trends Cogn Sci* 23:87–101.

809 Flores FJ, Hartnack KE, Fath AB, Kim S-E, Wilson MA, Brown EN, Purdon PL (2017)
810 Thalamocortical synchronization during induction and emergence from propofol-induced
811 unconsciousness. *Proc Natl Acad Sci U S A* 114:E6660–E6668.

812 Fries P (2015) Rhythms for Cognition: Communication through Coherence. *Neuron* 88:220–
813 235.

814 Fries P, Reynolds JH, Rorie AE, Desimone R (2001) Modulation of oscillatory neuronal
815 synchronization by selective visual attention. *Science* 291:1560–1563.

816 Fries P, Womelsdorf T, Oostenveld R, Desimone R (2008) The effects of visual stimulation and
817 selective visual attention on rhythmic neuronal synchronization in macaque area V4. *J*
818 *Neurosci* 28:4823–4835.

819 Friston KJ, Bastos AM, Pinotsis D, Litvak V (2015) LFP and oscillations—what do they tell us?
820 Current Opinion in Neurobiology 31:1–6 Available at:
821 <http://dx.doi.org/10.1016/j.conb.2014.05.004>.

822 Gao R, Peterson EJ, Voytek B (2017) Inferring synaptic excitation/inhibition balance from field
823 potentials. *Neuroimage* 158:70–78.

824 Geller AS, Burke JF, Sperling MR, Sharan AD, Litt B, Baltuch GH, Lucas TH 2nd, Kahana MJ
825 (2014) Eye closure causes widespread low-frequency power increase and focal gamma
826 attenuation in the human electrocorticogram. *Clin Neurophysiol* 125:1764–1773.

827 Gregoriou GG, Gotts SJ, Zhou H, Desimone R (2009) High-frequency, long-range coupling
828 between prefrontal and visual cortex during attention. *Science* 324:1207–1210.

829 Haegens S, Nácher V, Luna R, Romo R, Jensen O (2011) α -Oscillations in the monkey
830 sensorimotor network influence discrimination performance by rhythmical inhibition of
831 neuronal spiking. *Proc Natl Acad Sci U S A* 108:19377–19382.

832 Haider B, Schulz DPA, Häusser M, Carandini M (2016) Millisecond Coupling of Local Field
833 Potentials to Synaptic Currents in the Awake Visual Cortex. *Neuron* 90:35–42.

834 Henrie JA, Shapley R (2005) LFP power spectra in V1 cortex: the graded effect of stimulus
835 contrast. *J Neurophysiol* 94:479–490.

836 Hoppensteadt FC, Izhikevich EM (1998) Thalamo-cortical interactions modeled by weakly
837 connected oscillators: could the brain use FM radio principles? *Biosystems* 48:85–94.

838 Isaacson JS, Scanziani M (2011) How Inhibition Shapes Cortical Activity. *Neuron* 72:231–243
839 Available at: <http://dx.doi.org/10.1016/j.neuron.2011.09.027>.

840 Jensen O, Mazaheri A (2010) Shaping functional architecture by oscillatory alpha activity: gating
841 by inhibition. *Front Hum Neurosci* 4:186.

842 Jensen O, Tesche CD (2002) Frontal theta activity in humans increases with memory load in a
843 working memory task. *European Journal of Neuroscience* 15:1395–1399 Available at:
844 <http://dx.doi.org/10.1046/j.1460-9568.2002.01975.x>.

845 Johansson M (1999) The hilbert transform. Mathematics Master's Thesis Växjö University,
846 Suecia Disponible en internet: http://w3.msi.vxu.se/exarb/mj_ex.pdf, consultado el 19
847 Available at: <http://www.fuchs-braun.com/media/d9140c7b3d5004fbffff8007fffff0.pdf>.

848 Jones SR (2016) When brain rhythms aren't "rhythmic": implication for their mechanisms and
849 meaning. *Current Opinion in Neurobiology* 40:72–80 Available at:
850 <http://dx.doi.org/10.1016/j.conb.2016.06.010>.

851 Kasdin NJ (1995) Discrete simulation of colored noise and stochastic processes and $1/f^{\alpha}$ power law noise generation. *Proceedings of the IEEE* 83:802–827 Available at:
852 <http://dx.doi.org/10.1109/5.381848>.

853

854 Katzner S, Nauhaus I, Benucci A, Bonin V, Ringach DL, Carandini M (2009) Local Origin of
855 Field Potentials in Visual Cortex. *Neuron* 61:35–41 Available at:
856 <http://dx.doi.org/10.1016/j.neuron.2008.11.016>.

857 Khamechian MB, Kozyrev V, Treue S, Esgaie M, Daliri MR (2019) Routing information flow by
858 separate neural synchrony frequencies allows for “functionally labeled lines” in higher
859 primate cortex. *Proceedings of the National Academy of Sciences* 116:12506–12515
860 Available at: <http://dx.doi.org/10.1073/pnas.1819827116>.

861 Kirov R, Weiss C, Siebner HR, Born J, Marshall L (2009) Slow oscillation electrical brain
862 stimulation during waking promotes EEG theta activity and memory encoding. *Proc Natl
863 Acad Sci U S A* 106:15460–15465.

864 Le Van Quyen M, Foucher J, Lachaux J, Rodriguez E, Lutz A, Martinerie J, Varela FJ (2001)
865 Comparison of Hilbert transform and wavelet methods for the analysis of neuronal
866 synchrony. *J Neurosci Methods* 111:83–98.

867 Lindén H, Tetzlaff T, Potjans TC, Pettersen KH, Grün S, Diesmann M, Einevoll GT (2011)
868 Modeling the spatial reach of the LFP. *Neuron* 72:859–872.

869 Linkenkaer-Hansen K, Nikouline VV, Palva JM, Ilmoniemi RJ (2001) Long-range temporal
870 correlations and scaling behavior in human brain oscillations. *J Neurosci* 21:1370–1377.

871 Lisman JE, Idiart MA (1995) Storage of 7 ± 2 short-term memories in oscillatory subcycles.
872 *Science* 267:1512–1515.

873 Logothetis NK (2003) The Underpinnings of the BOLD Functional Magnetic Resonance Imaging
874 Signal. The Journal of Neuroscience 23:3963–3971 Available at:
875 <http://dx.doi.org/10.1523/jneurosci.23-10-03963.2003>.

876 Lundqvist M, Herman P, Warden MR, Brincat SL, Miller EK (2018) Gamma and beta bursts
877 during working memory readout suggest roles in its volitional control. *Nat Commun* 9:394.

878 Lu Y, Truccolo W, Wagner FB, Vargas-Irwin CE, Ozden I, Zimmermann JB, May T, Agha NS,
879 Wang J, Nurmikko AV (2015) Optogenetically induced spatiotemporal gamma oscillations
880 and neuronal spiking activity in primate motor cortex. *J Neurophysiol* 113:3574–3587.

881 Marple L (1999) Computing the discrete-time“ analytic” signal via FFT. *IEEE Trans Signal
882 Process* 47:2600–2603.

883 Martin KAC, Schröder S (2016) Phase Locking of Multiple Single Neurons to the Local Field
884 Potential in Cat V1. *J Neurosci* 36:2494–2502.

885 McGinley MJ, David SV, McCormick DA (2015) Cortical Membrane Potential Signature of
886 Optimal States for Sensory Signal Detection. *Neuron* 87:179–192.

887 Miller KJ, Sorensen LB, Ojemann JG, den Nijs M (2009) Power-law scaling in the brain surface
888 electric potential. *PLoS Comput Biol* 5:e1000609.

889 Milstein J, Mormann F, Fried I, Koch C (2009) Neuronal shot noise and Brownian 1/f² behavior
890 in the local field potential de la Prida LM, ed. *PLoS One* 4:e4338.

891 Misselhorn J, Schwab BC, Schneider TR, Engel AK (2019) Synchronization of Sensory Gamma
892 Oscillations Promotes Multisensory Communication. *eNeuro* 6 Available at:
893 <http://dx.doi.org/10.1523/ENEURO.0101-19.2019>.

894 Muller L, Piantoni G, Koller D, Cash SS, Halgren E, Sejnowski TJ (2016) Rotating waves during
895 human sleep spindles organize global patterns of activity that repeat precisely through the
896 night. *Elife* 5 Available at: <http://dx.doi.org/10.7554/eLife.17267>.

897 Muller L, Reynaud A, Chavane F, Destexhe A (2014) The stimulus-evoked population response
898 in visual cortex of awake monkey is a propagating wave. *Nat Commun* 5:3675.

899 Muria TTK, Aviyente S (2019) Time-Frequency Based Phase-Amplitude Coupling Measure For
900 Neuronal Oscillations. *Sci Rep* 9:12441.

901 Panagiotaropoulos TI, Deco G, Kapoor V, Logothetis NK (2012) Neuronal discharges and
902 gamma oscillations explicitly reflect visual consciousness in the lateral prefrontal cortex.
903 *Neuron* 74:924–935.

904 Panzeri S, Brunel N, Logothetis NK, Kayser C (2010) Sensory neural codes using multiplexed
905 temporal scales. *Trends Neurosci* 33:111–120.

906 Pereda E, Gamundi A, Rial R, González J (1998) Non-linear behaviour of human EEG: fractal
907 exponent versus correlation dimension in awake and sleep stages. *Neurosci Lett* 250:91–
908 94.

909 Pesaran B, Pezaris JS, Sahani M, Mitra PP, Andersen RA (2002) Temporal structure in
910 neuronal activity during working memory in macaque parietal cortex. *Nat Neurosci* 5:805–
911 811.

912 Pesaran B, Vinck M, Einevoll GT, Sirota A, Fries P, Siegel M, Truccolo W, Schroeder CE,
913 Srinivasan R (2018) Investigating large-scale brain dynamics using field potential
914 recordings: analysis and interpretation. *Nat Neurosci* 21:903–919.

915 Petersen CCH, Hahn TTG, Mehta M, Grinvald A, Sakmann B (2003) Interaction of sensory
916 responses with spontaneous depolarization in layer 2/3 barrel cortex. *Proc Natl Acad Sci U*
917 *S A* 100:13638–13643.

918 Poo C, Isaacson JS (2009) Odor representations in olfactory cortex: “sparse” coding, global
919 inhibition, and oscillations. *Neuron* 62:850–861.

920 Purdon PL, Pierce ET, Mukamel EA, Prerau MJ, Walsh JL, Wong KFK, Salazar-Gomez AF,
921 Harrell PG, Sampson AL, Cimenser A, Ching S, Kopell NJ, Tavares-Stoeckel C, Habeeb K,
922 Merhar R, Brown EN (2013) Electroencephalogram signatures of loss and recovery of
923 consciousness from propofol. *Proc Natl Acad Sci U S A* 110:E1142–E1151.

924 Ray S, Crone NE, Niebur E, Franaszczuk PJ, Hsiao SS (2008a) Neural correlates of high-
925 gamma oscillations (60-200 Hz) in macaque local field potentials and their potential
926 implications in electrocorticography. *J Neurosci* 28:11526–11536.

927 Ray S, Hsiao SS, Crone NE, Franaszczuk PJ, Niebur E (2008b) Effect of stimulus intensity on
928 the spike-local field potential relationship in the secondary somatosensory cortex. *J*
929 *Neurosci* 28:7334–7343.

930 Ray S, Maunsell JHR (2010) Differences in gamma frequencies across visual cortex restrict
931 their possible use in computation. *Neuron* 67:885–896.

932 Ray S, Maunsell JHR (2011) Different origins of gamma rhythm and high-gamma activity in
933 macaque visual cortex. *PLoS Biol* 9:e1000610.

934 Rubino D, Robbins KA, Hatsopoulos NG (2006) Propagating waves mediate information
935 transfer in the motor cortex. *Nat Neurosci* 9:1549–1557.

936 Sanes JN, Donoghue JP (1993) Oscillations in local field potentials of the primate motor cortex
937 during voluntary movement. *Proc Natl Acad Sci U S A* 90:4470–4474.

938 Scheffer-Teixeira R, Tort AB (2016) On cross-frequency phase-phase coupling between theta
939 and gamma oscillations in the hippocampus. *eLife* 5 Available at:
940 <http://dx.doi.org/10.7554/eLife.20515>.

941 Singer W, Gray CM (1995) Visual feature integration and the temporal correlation hypothesis.
942 *Annu Rev Neurosci* 18:555–586.

943 Souza BC, Tort ABL (2017) Asymmetry of the temporal code for space by hippocampal place
944 cells. *Sci Rep* 7:8507.

945 Steriade M, Timofeev I, Grenier F (2001) Natural Waking and Sleep States: A View From Inside
946 Neocortical Neurons. *Journal of Neurophysiology* 85:1969–1985 Available at:
947 <http://dx.doi.org/10.1152/jn.2001.85.5.1969>.

948 Strüber M, Sauer J-F, Bartos M (2022) Parvalbumin expressing interneurons control spike-
949 phase coupling of hippocampal cells to theta oscillations. *Sci Rep* 12:1362.

950 Takahashi M, Nishida H, Redish AD, Lauwereyns J (2014) Theta phase shift in spike timing and
951 modulation of gamma oscillation: a dynamic code for spatial alternation during fixation in rat
952 hippocampal area CA1. *J Neurophysiol* 111:1601–1614.

953 Teleńczuk B, Dehghani N, Le Van Quyen M, Cash SS, Halgren E, Hatsopoulos NG, Destexhe
954 A (2017) Local field potentials primarily reflect inhibitory neuron activity in human and
955 monkey cortex. *Sci Rep* 7:40211.

956 Thut G, Miniussi C, Gross J (2012) The functional importance of rhythmic activity in the brain.
957 *Curr Biol* 22:R658–R663.

958 Tingley D, Alexander AS, Quinn LK, Chiba AA, Nitz D (2018) Multiplexed oscillations and phase
959 rate coding in the basal forebrain. *Sci Adv* 4:eaar3230.

960 van Kerkoerle T, Self MW, Dagnino B, Gariel-Mathis M-A, Poort J, van der Togt C, Roelfsema
961 PR (2014) Alpha and gamma oscillations characterize feedback and feedforward
962 processing in monkey visual cortex. *Proc Natl Acad Sci U S A* 111:14332–14341.

963 van Vugt MK, Schulze-Bonhage A, Litt B, Brandt A, Kahana MJ (2010) Hippocampal gamma
964 oscillations increase with memory load. *J Neurosci* 30:2694–2699.

965 Vinck M, Batista-Brito R, Knoblich U, Cardin JA (2015) Arousal and locomotion make distinct
966 contributions to cortical activity patterns and visual encoding. *Neuron* 86:740–754.

967 Voytek B, Kramer MA, Case J, Lepage KQ, Tempesta ZR, Knight RT, Gazzaley A (2015) Age-
968 Related Changes in 1/f Neural Electrophysiological Noise. *J Neurosci* 35:13257–13265.

969 Wang X-J (2010) Neurophysiological and computational principles of cortical rhythms in
970 cognition. *Physiol Rev* 90:1195–1268.

971 Womelsdorf T, Schoffelen J-M, Oostenveld R, Singer W, Desimone R, Engel AK, Fries P (2007)
972 Modulation of Neuronal Interactions Through Neuronal Synchronization. *Science*
973 316:1609–1612 Available at: <http://dx.doi.org/10.1126/science.1139597>.

974 Worden MS, Foxe JJ, Wang N, Simpson GV (2000) Anticipatory biasing of visuospatial
975 attention indexed by retinotopically specific alpha-band electroencephalography increases
976 over occipital cortex. *J Neurosci* 20:RC63.

977 Yael D, Vecht JJ, Bar-Gad I (2018) Filter-Based Phase Shifts Distort Neuronal Timing
978 Information. *eNeuro* 5 Available at: <http://dx.doi.org/10.1523/ENEURO.0261-17.2018>.

979 Yu J, Ferster D (2010) Membrane potential synchrony in primary visual cortex during sensory
980 stimulation. *Neuron* 68:1187–1201.

981 Zanos TP, Mineault PJ, Pack CC (2011) Removal of spurious correlations between spikes and
982 local field potentials. *J Neurophysiol* 105:474–486.

983 Zareian B, Maboudi K, Daliri MR, Abrishami Moghaddam H, Treue S, Esghaei M (2020)
984 Attention strengthens across-trial pre-stimulus phase coherence in visual cortex, enhancing
985 stimulus processing. *Sci Rep* 10:4837.

986 Zutshi I, Brandon MP, Fu ML, Donegan ML, Leutgeb JK, Leutgeb S (2018) Hippocampal Neural
987 Circuits Respond to Optogenetic Pacing of Theta Frequencies by Generating Accelerated
988 Oscillation Frequencies. *Curr Biol* 28:1179–1188.e3.

989 **Figures**

990 **Figure 1. Cortical LFP recordings are inherently broad spectrum** **(a)** Spikes and local field
991 potentials (LFP) were recorded from area MT of common marmosets while they held fixation
992 on a blank screen. 3 seconds of raw LFP (filtered 1-100 Hz) and spike times from a well
993 isolated neuron recorded on the same electrode is plotted on the right. The red box indicates a
994 period of fixation during the recording epoch. **(b)** The power spectrum for the LFP trace in (a) is
995 plotted in black. 10 additional 3 second epochs are plotted in grey. The red dashed line is the
996 mean power spectrum across trials. **(c)** The raw LFP during fixation is plotted in black against
997 the narrowband filtered theta oscillatory component (4-8 Hz, red dotted line). **(d, e, f**, same as
998 **c**, but for alpha (8-15 Hz), beta (15-30 Hz), and low gamma (30-50 Hz) band pass filters. **(g)**
999 The wideband filtered (5-50 Hz) LFP follows the dominant fluctuation in the raw LFP as it shifts
1000 in temporal frequency.

1001

1002 **Figure 2. Spikes are more strongly coupled to the phase of wideband filtered LFP**
1003 **signals than narrowband oscillatory components. (a)** The raw (5-200 Hz) filtered LFP trace
1004 from Figure 1 is plotted in black. The wideband filtered trace (5-50 Hz) is plotted in pseudocolor
1005 corresponding to the generalized phase (GP) of the wideband filtered trace according to the
1006 color wheel. GP captures the troughs (blue/purple) and peaks (yellow/green) of the dominant
1007 fluctuations while interpolating over the higher frequency, lower amplitude riding cycles. **(b)**
1008 Histogram showing the fraction of spikes that occurred during different phases of the wideband
1009 filtered LFP (10 phase bins, N = 20 sessions across 2 monkeys; error bars indicate S.E.M.) **(c)**
1010 The spike-phase distribution was flatter for theta band (4-8 Hz) filtered LFP. The mean spike-
1011 phase index (SPI), which quantifies the mean vector length of the circular distribution of spike
1012 phases, is plotted across 20 sessions from 2 monkeys. The wideband filtered LFP (blue) had
1013 significantly stronger SPI values than theta filtered LFP (red; $p < 1 \times 10^{-9}$, two-tailed paired
1014 sample t-test) **(d-f)** Same as c, but for alpha (green; $p < 1 \times 10^{-10}$), beta (pink, $p < 1 \times 10^{-11}$), and
1015 gamma filtered LFP (green; $p < 1 \times 10^{-9}$).

1016

1017 **Figure 3. Stronger wideband spike-phase coupling is consistent across the population**
1018 **of recorded single-units. (a)** Scatter plot comparing the magnitude of SPI after use of a
1019 broadband filter (x-axis) or theta band filter (y-axis) for each identified single unit (N = 107
1020 across 20 recordings sessions). **(b-d)** Same as for (a) but for alpha, beta, and gamma filters.
1021 The wideband filter had a consistently stronger SPI than the narrowband filtered oscillatory
1022 phases across the population of single-units.

1023

1024 **Figure 4. Narrowband signals do not contain more spike-phase information. (a)** SPI
1025 values after restricting the inclusion of spikes to when significant power is present in each
1026 individual filter band (-5 dB SNR threshold, percentages indicate fraction of data above
1027 threshold; colored dots are N = 20 sessions from 2 monkeys; black dots are the population

1028 mean). **(b)** Representative ROC curves for GLM analyses comparing model sensitivity for
1029 identifying spike times based on phase, computed in four narrowband frequency ranges that
1030 tile the frequency space from 4-50 Hz (red), a single measure of narrowband oscillatory phase
1031 (blue), or the single wideband GP measure applied to the same frequency range as the 4-
1032 factor GLM (black). There was no significant difference between the 4-factor and wideband
1033 models in identifying spike times based on phase (Wilcoxon signed-rank test, $p = 0.16$),
1034 whereas the single best narrowband model was significantly weaker (beta; $p = 0.00008$). **(c)**
1035 Scatter plot comparing the correlation between the raw LFP and the filtered LFP signal (y-axis)
1036 and the SPI after filtering (x-axis) in each filter band. There was a significant positive
1037 correlation between SPI and how similar the raw LFP was with the signal after filtering
1038 (Pearson's $r = 0.65$, $p < 1 \times 10^{-12}$). **(d)** SPI for a range of band pass filters ranging in high pass
1039 (lower band, 1-50 Hz) and low pass (upper band, 5-125 Hz). Each pixel is color coded with its
1040 average SPI across each recording session ($N = 20$ sessions from 2 monkeys). White pixels
1041 are filter combinations that have bandwidths less than 4 Hz. Black contour lines denote SPI
1042 intervals (0.02).

1043

1044 **Figure 5. Two alternative hypotheses regarding the relationship between spiking activity**
1045 **and LFP fluctuations. (a)** Signals generated under the hypothesis embedded narrowband
1046 fluctuations drive spiking activity. We generated a narrowband oscillatory fluctuation with power
1047 between 8 and 15 Hz. Spikes were generated with a Poisson spike generator coupled to a
1048 phase-dependent probability distribution with spikes more likely at π/π phases and less likely
1049 at 0 phases of the narrowband oscillation. This narrowband signal was added to randomly
1050 generated broadband noise to create a simulated LFP. **(b)** Signals generated under the
1051 hypothesis ensemble broadband fluctuations drive spiking activity. We generated the same
1052 narrowband oscillatory fluctuation and added the same randomly generated broadband noise
1053 as in the simulated LFP in a. Spikes were then generated as in (a), but to the phase of the

1054 broadband simulated LFP signal. **(c)** The result of the 2 signal generation paradigms is 2
1055 identical simulated LFP traces, but with different spike trains generated in relation to the state
1056 of either the narrow (blue raster) or broadband (red raster) signal. **(d)** The mean power
1057 spectrum across 20 simulated LFP signals (error bars are S.E.M).

1058

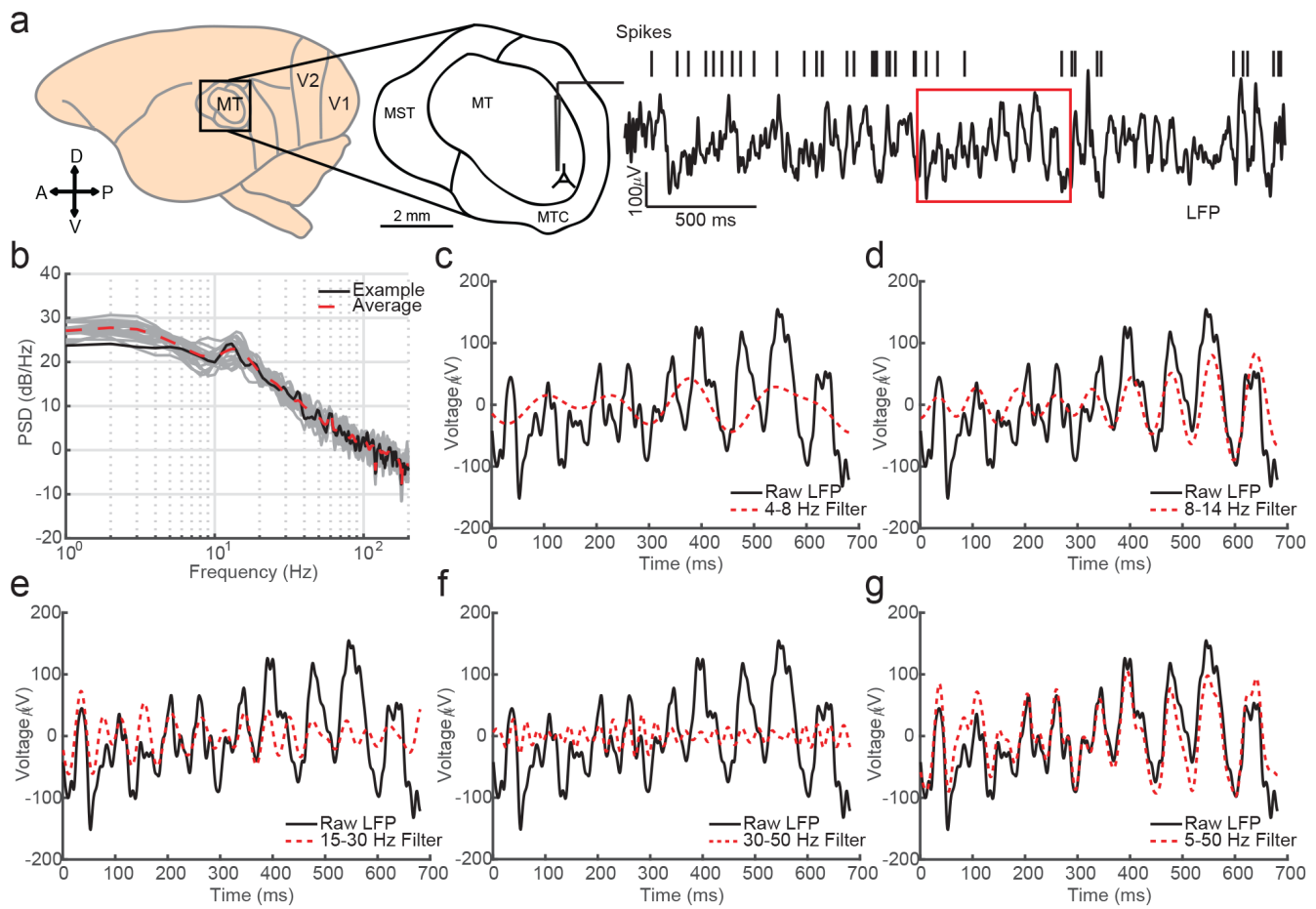
1059 **Figure 6. Spike-phase relationship is best recovered when the filter matches the signal**
1060 **(a)** The 8-15 Hz narrowband filtered LFP (solid blue line) is the recovered spike-generating
1061 signal from the ensemble simulated LFP (dotted blue line) under hypothesis A. **(b)** The SPI
1062 from the phase of the narrowband signal is significantly stronger after narrowband filtering as
1063 compared to wideband filtering for the simulation where spikes were coupled to the phase of
1064 the narrowband component (5-100 Hz; N = 20 simulations; $p < 0.0001$ two-tailed Wilcoxon
1065 signed-rank test). **(c)** The wideband filtered LFP (5-100 Hz, red line) is the recovered spike-
1066 generating signal from the broadband simulated LFP under hypothesis B (dotted red line). **(d)**
1067 The SPI from the phase of the wideband is significantly stronger after wideband filtering as
1068 compared to narrowband filtering for the simulation where spikes were coupled to the phase of
1069 the broadband LFP ($p < 0.0001$ two-tailed Wilcoxon signed-rank test).

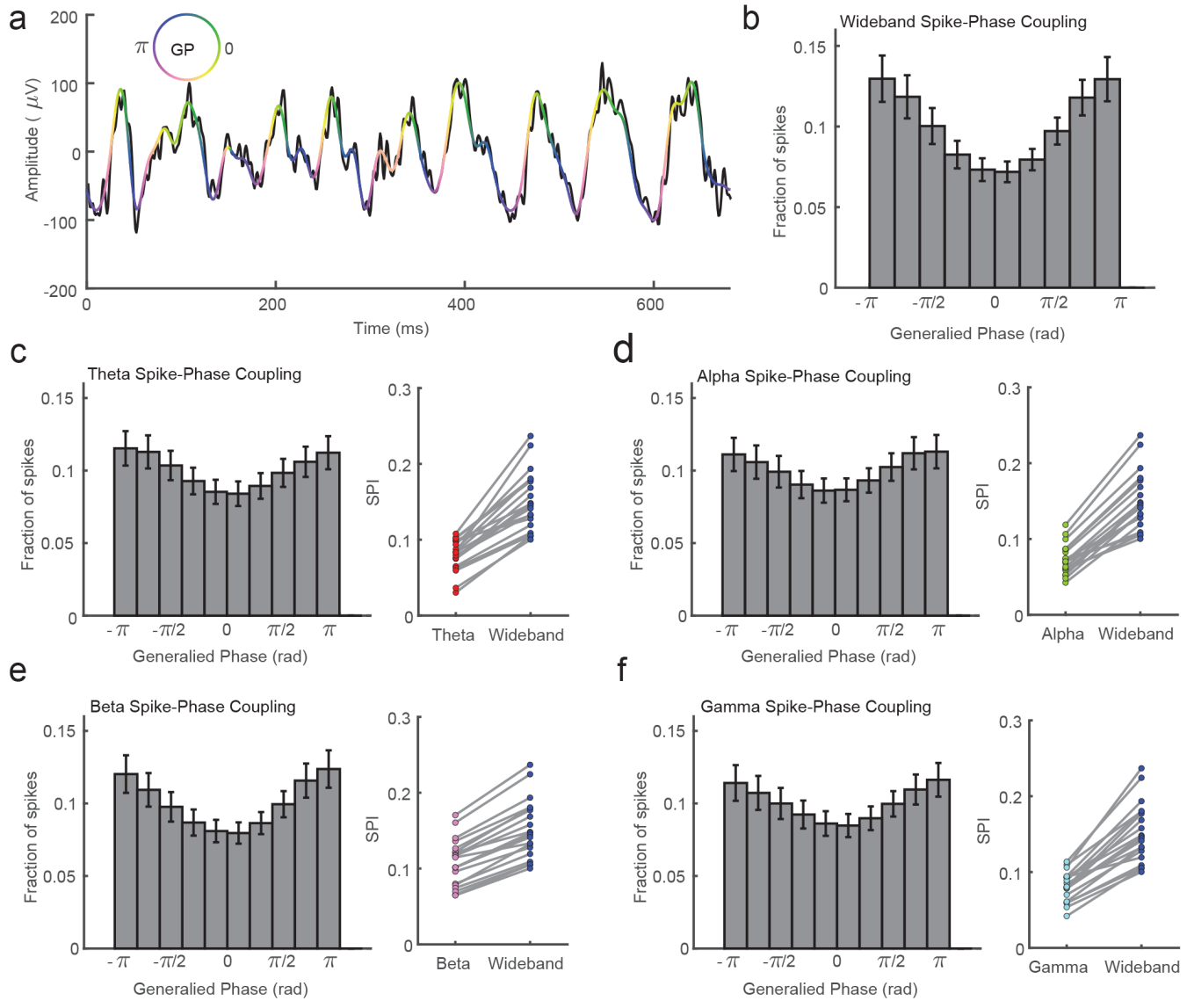
1070

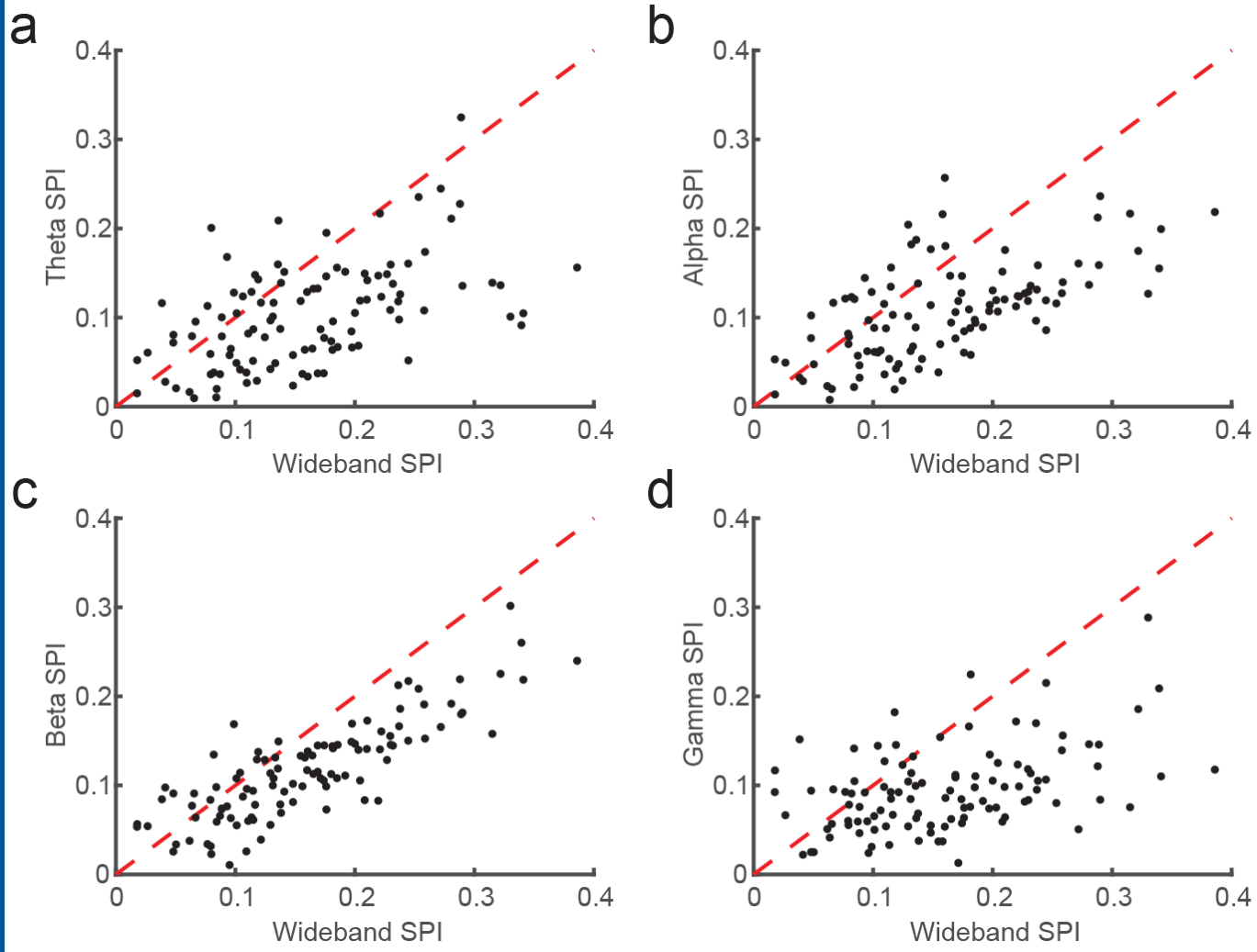
1071 **Figure 7. The model with a broadband spike correlation best matches cortical recordings.**

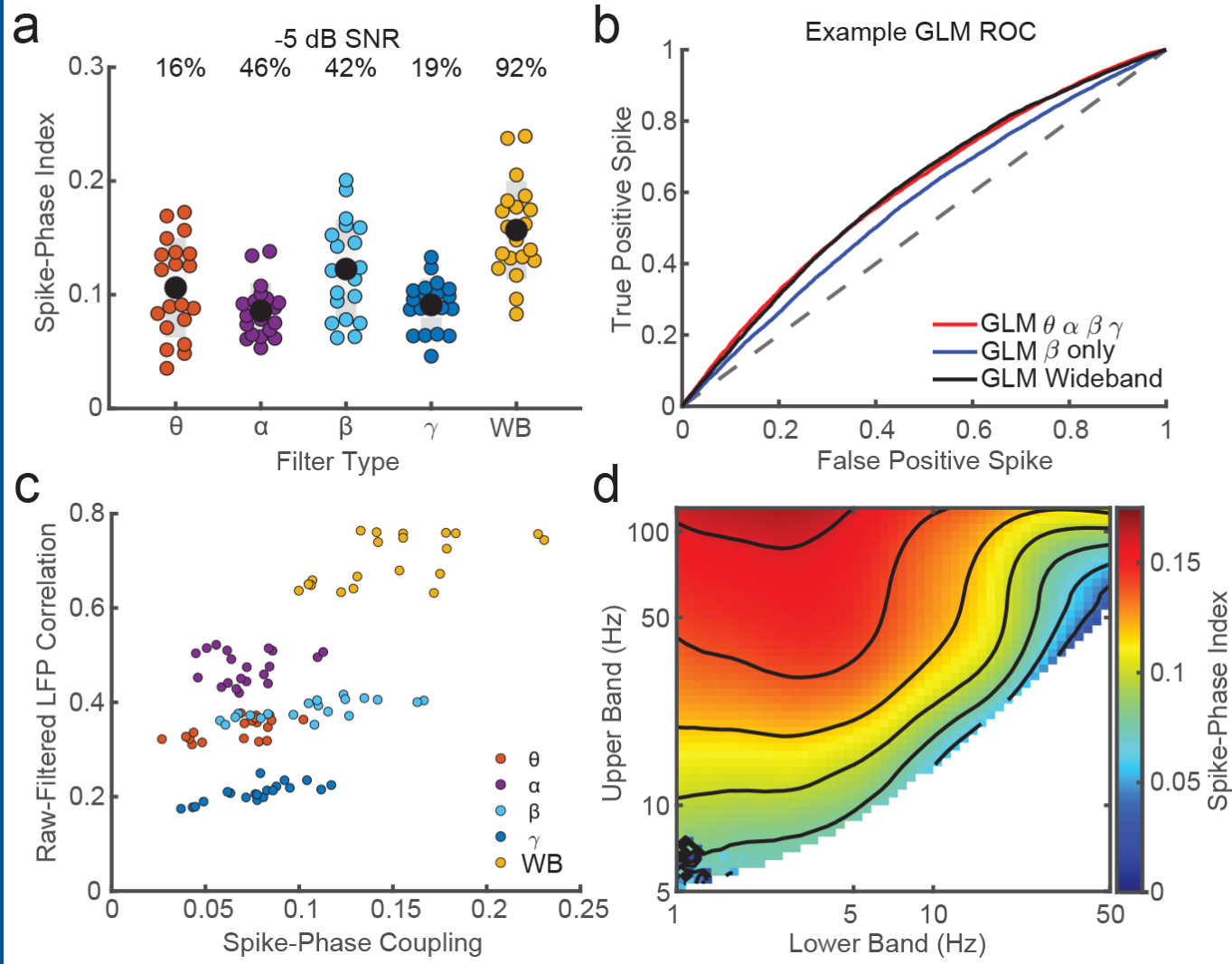
1072 **(a)** SPI values after filtering simulated LFP in various band passes when spike times are
1073 correlated to the phase of 8-15 Hz narrowband component. In this case, the optimal filter is
1074 aligned to the signal source (8-15 Hz). **(b)** Same as (a), but when spike times are coupled to the
1075 phase of the broadband LFP. The pattern of SPI across filters is well matched to the pattern
1076 observed in data (Figure 4c). **(c)** SPI (x-axis) is poorly correlated with the similarity between
1077 filtered and raw simulated LFP (y-axis) when spikes are correlated with narrowband signal
1078 phase (blue dots, $r^2 = 0.08$). Conversely, the correlation is strong when spikes are correlated

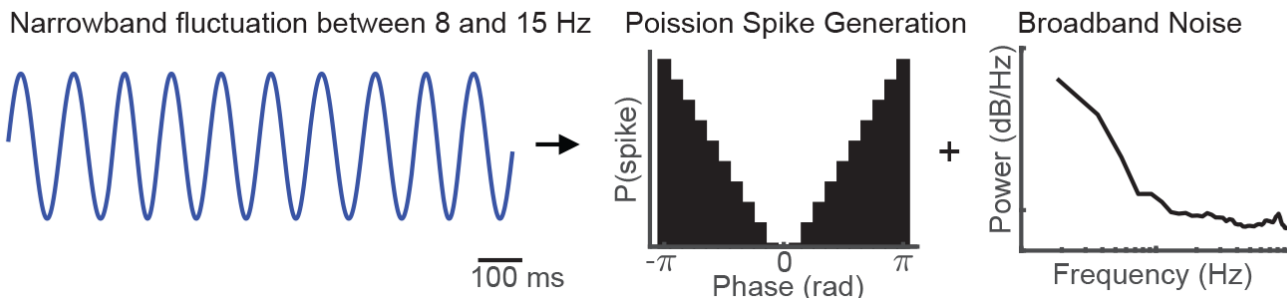
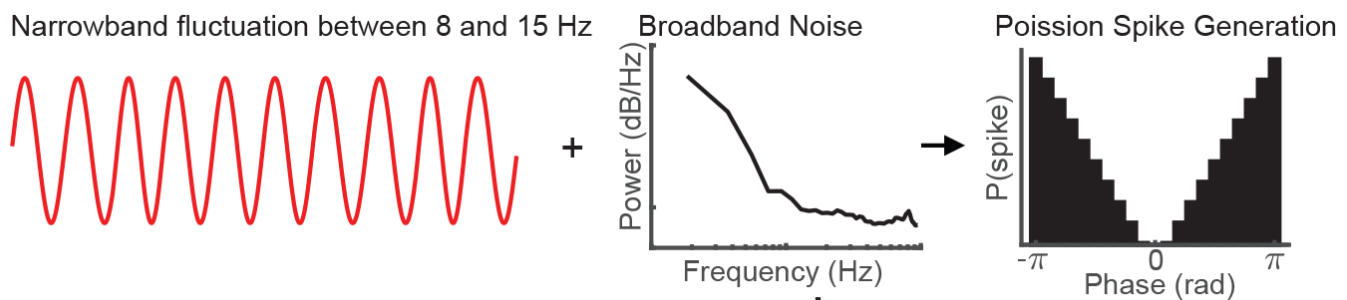
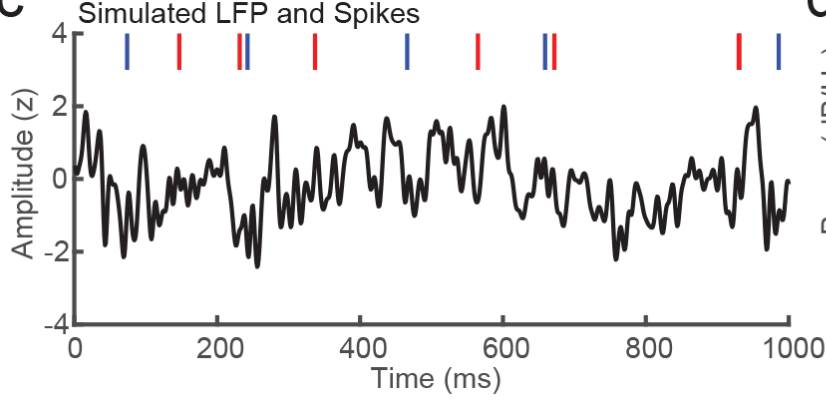
1079 with broad-band signal phase (red dots, $r^2 = 0.85$). The relationship for a broad-band signal
1080 source is well matched to the pattern observed in the cortical recordings (Figure 4c).









a Hypothesis 1: Neuronal activity coupled to narrowband component**b** Hypothesis 2: Neuronal activity coupled to broad spectrum**c** Simulated LFP and Spikes**d** Mean Simulated LFP PSD